Topological nonmagnetic impurity states in topological Kondo insulators

M. Abele, X. Yuan, and P. S. Riseborough
Physics Department, Temple University, Philadelphia, Pennsylvania 19122, USA

(Received 26 July 2019; accepted 18 February 2020; published 2 March 2020)

We examine the presence of nonmagnetic impurities in a hybridization gap model of a Kondo insulator which has band inversion. The model has been used to predict that SmB_6 is a topological insulator. We show that there are two types of nonmagnetic impurity states in a Kondo insulator. The type of states can be categorized as deep impurity states, similar to the impurity states in an ordinary metal, and impurity states which have energies within the hybridization gap. Unlike the deep impurity states which only form if the impurity potential exceeds a critical value of the order of the conduction bandwidth, the in-gap impurity states form for exceptionally small values of the impurity potential comparable to the hybridization gap. This result may explain why Kondo insulators are found to be exceptionally sensitive to impurities. We show that these in-gap states are caused by band inversion and have properties similar to those expected for impurities in a topological insulator.

DOI: 10.1103/PhysRevB.101.094101

I. INTRODUCTION

Kondo insulators are semiconductors that have extremely narrow gaps of the order of 10s–100s of meV which are thought to be hybridization gaps produced by the mixing of localized f and itinerant conduction band states [1,2]. The smallness of the gap is generally attributed to a renormalization of the hybridization process by strong Coulomb interactions between the f electrons [3]. It has been predicted that the cubic material SmB_6 is a time-reversal inversion symmetric topological Kondo insulator [4,5]. There are five different classifications of three-dimensional (3D) topological insulators, as shown in Ref. [6]. An insulator with cubic symmetry falls into the topologically nontrivial (Z_2) class if it is time-reversal invariant and has inversion symmetry, and if an odd numbers of bands, with different parities, invert at an odd number of the four time-reversal invariant points Γ, R, X, and M of the Brillouin zone. The prediction of a nontrivial topological character of SmB_6 has motivated extensive investigation of the properties of SmB_6 and is consistent with the long-known finding [7–9] that that the resistivity shows thermally activated behavior which plateaus and saturates at temperatures below 4 K. The plateauing of the resistivity is consistent with the existence of surface states [10–13]. Transport measurements, using a Corbino geometry [14], have separated out the bulk resistivity from the surface contribution [15]. The bulk component of the resistivity is thermally activated and increases by ten orders of magnitude [15], indicating that the bulk is an exceptionally good insulator and that the surface is metallic. Surface states have also been observed in ARPES [16–18] and tunneling spectroscopies [19–24], which provides further evidence that is consistent with SmB_6 being topological. However, despite a number of experimental efforts by various groups, no direct evidence has been obtained which conclusively proves that SmB_6 has a nontrivial gauge topological.

The properties of SmB_6 are not well understood, probably partially due to the strong electronic correlations [19,21,25–29] and probably due to the presence of impurities [30–35]. For example, the Fermi velocities of the surface states that were inferred from different measurement techniques [16,36,37] differ by three orders of magnitude. Magnetotransport measurements show a puzzling hysteretic behavior [38]. The material shows a linear T term in the specific heat which has a coefficient that varies between 2 and 25 mJ/mol K^{-2}, depending upon the sample preparation [32–35]. Doping with 5% of magnetic impurities can lead to an order of magnitude increase in the heat capacity [39]. Likewise, large linear T terms in the thermal conductivity have been reported in some samples [40,41], but are absent in other well-characterized samples [42,43]. Despite the very high resistance of the bulk, optical conductivity in the THz frequency range measured in transmission mode [44] shows an extremely large conductivity indicating the existence of localized in-gap states, but was unable to determine whether the AC conductivity was due to surface or bulk states. It has been shown theoretically that f vacancies in Kondo insulators produce in-gap bound states [45] and that only a small concentration of about 4% of vacancies is sufficient to close the hybridization gap [46]. Raman scattering experiments [47] show that as few as 1% vacancies may close the gap. There are reports of unusual high-frequency quantum oscillations found in some samples that have been claimed to have their origin in the bulk [40]. These results have not been reproduced by other groups [37,48,49], and it has been suggested [50] that the oscillations may have an extrinsic origin. This suggestion that the unusual oscillations have an extrinsic origin is consistent with the large values of the linear-T coefficient in the specific heat and thermal conductivity that were reported along with the oscillations [40,41]. The question has arisen whether the in-gap states are intrinsic or extrinsic.

Here we shall consider the effects of nonmagnetic impurities in Kondo insulators and show that they can support two types of nonmagnetic impurity states, and that the in-gap states may be topologically nontrivial. The other types of impurity states are topologically trivial. Our calculations

are restricted to nonmagnetic impurities, though experimental suggests that magnetic impurities [39,51] may lead to a novel type of Kondo effect. In our calculations, when a f vacancy is created, the on-site f level energy is removed to higher energies and no longer participates in a coherent hybridization process. Since the categorization of SmB_6 as having nontrivial topology depends on the relative energies of the E_f level and the three time-reversal invariant X points in the conduction band [4], a shift of E_f in a finite volume of space may result in a change of topology and the formation of topologically protected surface states.

A rationalization of our finding is given by consideration of an isolated vacancy as being adiabatically connected to a void in a topological insulator. As shown in Appendix A, a void in a topological insulator can be modeled by the Dirac equation with a spatially dependent mass [52–54] which changes sign. Changing the sign of the mass in the Dirac equation produces a change in parity of the eigenfunctions and results in a change in the winding number. Voids with sufficiently large ratios of the magnitudes of the masses and sufficiently large radii have their own surface states that have topological characters similar to those of topological surface states on the exterior of the crystal. The surface states of a spherical void are characterized by their total angular momentum (j, j_z) and the parity eigenvalue of the upper components of the Dirac equation. The void surface states are in-gap surface states and have only half the degrees of freedom of the bulk states. This is analogous to the reduction of the degrees of freedom in the bulk of a three-dimensional bulk topological insulator that occurs at a planar surface, which leads to spin-momentum locking. Also shown in Appendix A, for a thin film of a topological insulator, tunneling between the front surface and the back surface can produce an exponentially small gap in the surface state dispersion relation [55,56] and can destroy spin-momentum locking. We argue that an impurity can be modeled by adiabatically continuing the void radii to arbitrarily small values, but also continuing the mass ratios to arbitrarily large values which suppresses tunneling across the vacancy. Hence, in this limit, the in-gap impurity states produced by a vacancy in a TI are expected to be similar to the surface states on the exterior of a topological insulator. In fact, as has been previously shown by Sollie and Schlottmann [45], an isolated vacancy does produce an in-gap state of f character, but instead of being localized at the vacancy site is spread equally over the surrounding nearest neighbor shell of atoms. Here we reexamine the model in more detail and show that the formation of an in-gap impurity state involves the same ingredients, namely band inversion by hybridization and strong spin-orbit coupling, that are required for the creation of the topologically nontrivial surface states in a topological Kondo insulator [4].

II. THE HAMILTONIAN

We shall consider the effects of nonmagnetic impurities within a quasiparticle picture. Using a slave boson mean-field theory [3], one finds renormalized bands with an effective hybridization matrix element $V \to V\sqrt{1-n_f}$ that mixes the bands with different orbital characters, an effective f level energy $E_f + \lambda$ which is shifted towards the chemical potential, and a renormalized indirect hybridization gap $V^2/W(1-n_f)$ in which n_f is the f occupancy. For SmB_6, the indirect hybridization gap is estimated to be of the order of 20 meV. The renormalization of the quasiparticle bands is accompanied by a reduction in the f quasiparticle weight, as has also been found in other models of strongly correlated topological insulators using DMFT [57]. Furthermore, an investigation using an inhomogeneous version of the slave boson method that models a surface layer of a Kondo insulator by setting the slave boson amplitude to zero [58], finds that at $T = 0$ the hybridization on the layer next to the surface is only reduced by about 30%. The authors of Ref. [58] posit that the the intervention of magnetism or other instabilities may prevent the establishment of the Kondo effect at $T = 0$. Similar calculations presented in Appendix B are in complete accord with the findings of Alexandrov *et al.* [58] since they indicate that the $T = 0$ Fermi liquid and topological characters of the material are preserved in the presence of Coulomb correlations, in the absence of intervening phase transitions.

The quasiparticle picture maps onto the noninteracting Hamiltonian introduced by Sollie and Schlottmann [45],

$$\hat{H} = \hat{H}_0 + \hat{H}_I, \tag{1}$$

where $\hat{H}_0$ describes a homogeneous electronic system described by the Anderson lattice model

$$\hat{H}_0 = \sum_{\underline{k},\alpha} (\epsilon(\underline{k}) d^\dagger_{\underline{k},\alpha} d_{\underline{k},\alpha} + E_{f,\alpha} f^\dagger_{\underline{k},\alpha} f_{\underline{k},\alpha}) + \sum_{\underline{k},\alpha} (V(\underline{k}) f^\dagger_{\underline{k},\alpha} d_{\underline{k},\alpha} + V^*(\underline{k}) d^\dagger_{\underline{k},\alpha} f_{\underline{k},\alpha}), \tag{2}$$

where the degeneracy index α takes on D_α values. The term $\hat{H}_I$ describes the potential due to an impurity nucleus located at the origin $\underline{R} = 0$,

$$\hat{H}_I = \frac{1}{N} \sum_{\underline{k},\underline{k}',\alpha} \Delta U f^\dagger_{\underline{k},\alpha} f_{\underline{k}',\alpha}, \tag{3}$$

in which N is the number of lattice sites. The energy $\epsilon(\underline{k})$ is the energy eigenvalue for a conduction band Bloch state of wave vector $\underline{k}$. The unhybridized conduction band density of states per site $\rho_{0,d}(\omega)$ has a width denoted by $2W$. The energy $E_{f,\alpha}$ is the binding energy of the f orbital labeled by α and $V(\underline{k})$ is the strength of the bulk hybridization energy. The bulk hybridization strength $V(\underline{k})$ is an odd function of $\underline{k}$, since we assume that the f and conduction bands have opposite parities. In general, the hybridization has a form $V(\underline{k}) = \underline{d}(\underline{k}) \cdot \underline{\sigma}$ [4] and, so, is only expected to vanish at isolated points. The density of states of the pure system is expected to exhibit an indirect hybridization gap of order $|V|^2/W$. The energy ΔU is the strength of the potential of the impurity on the f site. As will be shown later, ΔU is to be identified with the differences of binding energy of the f state on the impurity and the host f orbital.

A. The f-electron Green's functions

The time-dependent single-electron ff Green's function is defined as

$$G^{ff}_{\underline{k},\alpha;\underline{k}',\alpha'}(t) = -\frac{i}{\hbar} \langle \hat{T} f_{\underline{k},\alpha}(t) f^\dagger_{\underline{k}',\alpha'}(0) \rangle, \tag{4}$$

where $\hat{T}$ is Wick's time-ordering operator. The equations of motion are evaluated from

$$i\hbar\frac{\partial}{\partial t}G^{ff}_{\underline{k},\alpha;\underline{k}',\alpha'}(t) = \delta(t)\,\delta_{\underline{k},\underline{k}'}\,\delta_{\alpha,\alpha'} - \frac{i}{\hbar}\langle\hat{T}[f_{\underline{k},\alpha}(t),\hat{H}(t)]f^{\dagger}_{\underline{k}',\alpha'}(0)\rangle, \quad (5)$$

where the commutators can be evaluated in term of the df Green's function:

$$G^{df}_{\underline{k},\alpha;\underline{k}',\alpha'}(t) = -\frac{i}{\hbar}\langle\hat{T}\,d_{\underline{k},\alpha}(t)f^{\dagger}_{\underline{k}',\alpha'}(0)\rangle, \quad (6)$$

which satisfies a similar equation of motion. The Fourier transform of the ff-electron Green's function is defined as

$$G^{ff}_{\underline{k},\alpha;\underline{k}',\alpha'}(\omega) = \int_{-\infty}^{\infty} dt\,\exp[i\omega t]G^{ff}_{\underline{k},\alpha;\underline{k}',\alpha'}(t). \quad (7)$$

The poles of the Fourier transformed Green's functions represent the excitation energies of the system. The Fourier transformed Green's equations of motion form a closed algebraic set of equations of motion that consist of

$$(\omega - E_{f,\alpha})G^{ff}_{\underline{k},\alpha;\underline{k}',\alpha'}(\omega) = \delta_{\underline{k},\underline{k}'}\delta_{\alpha,\alpha'} + V(\underline{k})G^{df}_{\underline{k},\alpha;\underline{k}',\alpha'}(\omega) + \frac{1}{N}\sum_{\underline{k}''}\Delta U\; G^{ff}_{\underline{k}'',\alpha;\underline{k}',\alpha'}(\omega) \quad (8)$$

and

$$(\omega - \epsilon(\underline{k}))G^{df}_{\underline{k},\alpha;\underline{k}',\alpha'}(\omega) = V^{*}(\underline{k})G^{ff}_{\underline{k},\alpha;\underline{k}',\alpha'}(\omega). \quad (9)$$

The above equations can be combined to yield

$$\left(\omega - E_{f,\alpha} - \frac{|\,V(\underline{k})|^2}{\omega - \epsilon(\underline{k})}\right)G^{ff}_{\underline{k},\alpha;\underline{k}',\alpha'}(\omega) = \delta_{\underline{k},\underline{k}'}\delta_{\alpha,\alpha'} + \frac{1}{N}\sum_{\underline{k}''}\Delta U\,G^{ff}_{\underline{k}'',\alpha;\underline{k}',\alpha'}(\omega). \quad (10)$$

On defining the ff Green's function for the solid in the absence of the impurity, via

$$G^{f,0}_{\underline{k},\alpha}(\omega) = \frac{[\omega - \epsilon(\underline{k})]}{(\omega - E_{f,\alpha})[\omega - \epsilon(\underline{k})] - |V(\underline{k})|^2}, \quad (11)$$

one can solve for the ff Green's function in terms of the T matrix

$$G^{ff}_{\underline{k},\alpha;\underline{k}',\alpha}(\omega) = G^{f,0}_{\underline{k},\alpha}(\omega)\delta_{\underline{k},\underline{k}'} + G^{f,0}_{\underline{k},\alpha}(\omega)T_{\alpha}(\omega)G^{f,0}_{\underline{k}',\alpha}(\omega), \quad (12)$$

where the T matrix is calculated as

$$T_{\alpha}(\omega) = \frac{1}{N}\frac{\Delta U}{1 - \Delta U\frac{1}{N}\sum_{\underline{k}''}G^{f,0}_{\underline{k}'',\alpha}(\omega)}. \quad (13)$$

B. The *d*-electron Green's functions

The time-dependent single-electron dd Green's function is defined as

$$G^{dd}_{\underline{k},\alpha;\underline{k}',\alpha'}(t) = -\frac{i}{\hbar}\langle\hat{T}\,d_{\underline{k},\alpha}(t)d^{\dagger}_{\underline{k}',\alpha'}(0)\rangle. \quad (14)$$

Likewise, the fd Green's function is defined as

$$G^{fd}_{\underline{k},\alpha;\underline{k}',\alpha'}(t) = -\frac{i}{\hbar}\langle\hat{T}\,f_{\underline{k},\alpha}(t)d^{\dagger}_{\underline{k}',\alpha'}(0)\rangle. \quad (15)$$

The Fourier transformed dd-electron and fd Green's functions satisfy the coupled equations of motion

$$[\omega - \epsilon(\underline{k})]G^{dd}_{\underline{k},\alpha;\underline{k}',\alpha'}(\omega) = \delta_{\underline{k},\underline{k}'}\delta_{\alpha,\alpha'} + V^{*}(\underline{k})G^{fd}_{\underline{k},\alpha;\underline{k}',\alpha'}(\omega),$$
$$(\omega - E_{f,\alpha})G^{fd}_{\underline{k},\alpha;\underline{k}',\alpha'}(\omega) = V(\underline{k})G^{dd}_{\underline{k},\alpha;\underline{k}',\alpha'}(\omega) + \frac{1}{N}\sum_{\underline{k}''}\Delta U\,G^{fd}_{\underline{k}'',\alpha;\underline{k}',\alpha'}(\omega). \quad (16)$$

On defining the unperturbed dd-electron Green's function by

$$G^{dd,0}_{\underline{k},\alpha}(\omega) = \frac{(\omega - E_{f,\alpha})}{(\omega - E_{f,\alpha})[\omega - \epsilon(\underline{k})] - |V(\underline{k})|^2} \quad (17)$$

and the hybrid Green's function

$$G^{fd,0}_{\underline{k},\alpha}(\omega) = \frac{V(\underline{k})}{(\omega - E_{f,\alpha})[\omega - \epsilon(\underline{k})] - |V(\underline{k})|^2} \quad (18)$$

one finds that the dd-electron Green's function can be expressed in terms of the T matrix as

$$G^{dd}_{\underline{k},\alpha;\underline{k}',\alpha}(\omega) = \delta_{\underline{k},\underline{k}'}G^{dd,0}_{\underline{k},\alpha}(\omega) + G^{fd,0}_{\underline{k},\alpha}(\omega)^{*}T_{\alpha}(\omega)G^{fd,0}_{\underline{k}',\alpha}(\omega). \quad (19)$$

In the absence of the impurity potential ΔU and with $E_f = 0$, the model exhibits particle-hole symmetry. As will be seen below, this symmetry is broken for finite ΔU but the symmetry in the low-energy spectrum is restored for large $|\Delta U|$.

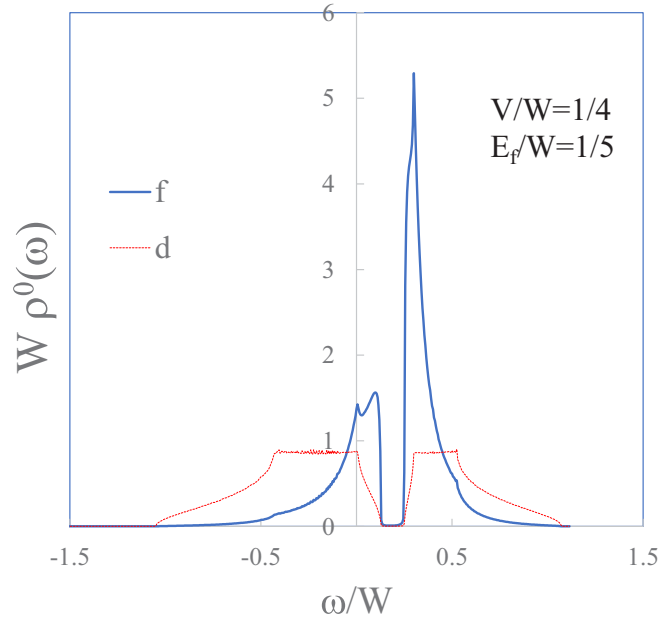

FIG. 1. The unperturbed f, $\rho^{0,f}(\omega)$ (blue), and d, $\rho^{0,d}(\omega)$ (red), hybridized density of states as a function of energy. The f-binding energy is $E_{f,\alpha} = W/5$ and hybridization matrix elements $V = W/4$. These values are not representative of SmB_6 but were chosen simply for clarity of illustration.

III. THE DENSITY OF STATES

The total density of states $\rho_T(\omega)$ can be expressed in terms of the trace of the Green's functions

$$\rho_T(\omega) = -\lim_{\eta\to 0}\frac{1}{\pi}\sum_{\underline{k},\alpha}\mathrm{Im}m\big(G^{ff}_{\underline{k},\alpha;\underline{k}',\alpha}(\omega+i\eta) + G^{dd}_{\underline{k},\alpha;\underline{k},\alpha}(\omega+i\eta)\big), \tag{20}$$

where $\eta\to 0+$. The density of states can be separated into the term $\rho^0_T(\omega)$ which represents the continuous density of states of states of the homogeneous system and $\Delta\rho_T(\omega)$ which represents the change in the density of states due to the presence of the impurity potential at the origin:

$$\rho_T(\omega) = \rho^0_T(\omega) + \Delta\rho_T(\omega). \tag{21}$$

The total density of states for the homogeneous system $\rho^0_T(\omega)$ can be expressed as

$$\rho^0_T(\omega) = N\sum_\alpha\left[1+\frac{|V|^2}{(\omega-E_{f,\alpha})^2}\right]\rho_{0,d}\left(\omega-\frac{|V|^2}{(\omega-E_{f,\alpha})}\right), \tag{22}$$

where $\rho_0(\omega)$ is the bulk conduction band density of states, per site, in the absence of hybridization. This density of states has the form of two hybridized bands, separated by a hybridization gap as is seen in Fig. 1. The change in the total density of states caused by the presence of the impurity is given by

$$\begin{aligned}\Delta\rho_T(\omega) &= \frac{1}{\pi}\sum_\alpha \mathrm{Im}\,m\left(\frac{\Delta U\frac{\partial}{\partial\omega}\frac{1}{N}\sum_{\underline{k}'}G^{f,0}_{\underline{k}',\alpha}(\omega+i\eta)}{1-\Delta U\frac{1}{N}\sum_{\underline{k}''}G^{f,0}_{\underline{k}'',\alpha}(\omega+i\eta)}\right)\\ &= -\frac{1}{\pi}\sum_\alpha\frac{\partial}{\partial\omega}\mathrm{Im}\,m\ln T_\alpha(\omega+i\eta)\\ &= -\frac{1}{\pi}\sum_\alpha\frac{\partial\delta_\alpha(\omega)}{\partial\omega},\end{aligned} \tag{23}$$

where $\delta(\omega)$ is the phase shift of the T matrix

$$T_\alpha(\omega) = |T_\alpha(\omega)|\exp[i\delta_\alpha(\omega)]. \tag{24}$$

This result is in accordance with Friedel's theorem [59]. The change in the density of states is shown in Fig. 2. The ω integral over $\Delta\rho_T(\omega)$ is zero since the total number of states in Hilbert space is conserved. The phase shift jumps by π at the position of the bound state, indicating that the impurity state has a total spectral weight of unity.

A. Bound state formation

In the limit of zero hybridization, the unperturbed f-electron Green's function reduces to

$$G^{f,0}_{\underline{k},\alpha}(\omega) = \frac{1}{\omega+i\eta-E_{f,\alpha}}. \tag{25}$$

Hence, the expression for $\Delta\rho_T(\omega)$ simplifies to

$$\begin{aligned}\lim_{V\to 0}\Delta\rho_T(\omega) &= -\frac{1}{\pi}\lim_{\eta\to 0}\sum_\alpha\mathrm{Im}\,m\left[\frac{\Delta U}{(\omega+i\eta-E_{f,\alpha}-\Delta U)(\omega+i\eta-E_{f,\alpha})}\right]\\ &= \lim_{\eta\to 0}\sum_\alpha\frac{1}{\pi}\frac{\eta}{(\omega-E_{f,\alpha}-\Delta U)^2+\eta^2}-\lim_{\eta\to 0}\sum_\alpha\frac{1}{\pi}\frac{\eta}{(\omega-E_{f,\alpha})^2+\eta^2}.\end{aligned} \tag{26}$$

This result corresponds to the production of a series of delta functions with weights plus or minus unity located at the energies

$$\begin{aligned}\omega &= E_{f,\alpha}+\Delta U,\\ \omega &= E_{f,\alpha}.\end{aligned} \tag{27}$$

The first corresponds to impurity bound states and the second to the removal of the localized f levels at the impurity site. The total number of states is preserved, in accordance with the conservation of the dimensionality of Hilbert space. The above analysis identifies ΔU with the difference of the f-binding energies of the f state of the impurity and the host f state.

The presence of hybridization drastically changes the above result. The hybridization introduces band inversion in the total density of states and produces an indirect hybridization gap. In general, the change in the total density of states caused by the impurity $\Delta\rho_T(\omega)$ can be written as

$$\begin{aligned}\Delta\rho_T(\omega) = \frac{1}{\pi}\sum_\alpha&\left[\frac{\frac{\Delta U}{N}\sum_{\underline{k}}\frac{\partial}{\partial\omega}\mathrm{Im}\,mG^{f,0}_{\underline{k},\alpha}(\omega)\big[1-\frac{\Delta U}{N}\sum_{\underline{k}'}\mathrm{Re}\,eG^{f,0}_{\underline{k}',\alpha}(\omega)\big]}{[1-\frac{\Delta U}{N}\sum_{\underline{k}''}\mathrm{Re}\,eG^{f,0}_{\underline{k}'',\alpha}(\omega)]^2+\big[\frac{\Delta U}{N}\sum_{\underline{k}''}\mathrm{Im}\,mG^{f,0}_{\underline{k}'',\alpha}(\omega)\big]^2}\right]\\ +\frac{1}{\pi}\sum_\alpha&\left[\frac{\frac{\Delta U}{N}\sum_{\underline{k}}\frac{\partial}{\partial\omega}\mathrm{Re}\,eG^{f,0}_{\underline{k},\alpha}(\omega)\big[\frac{\Delta U}{N}\sum_{\underline{k}'}\mathrm{Im}\,mG^{f,0}_{\underline{k}',\alpha}(\omega)\big]}{[1-\frac{\Delta U}{N}\sum_{\underline{k}''}\mathrm{Re}\,eG^{f,0}_{\underline{k}'',\alpha}(\omega)]^2+\big[\frac{\Delta U}{N}\sum_{\underline{k}''}\mathrm{Im}\,mG^{f,0}_{\underline{k}'',\alpha}(\omega)\big]^2}\right].\end{aligned} \tag{28}$$

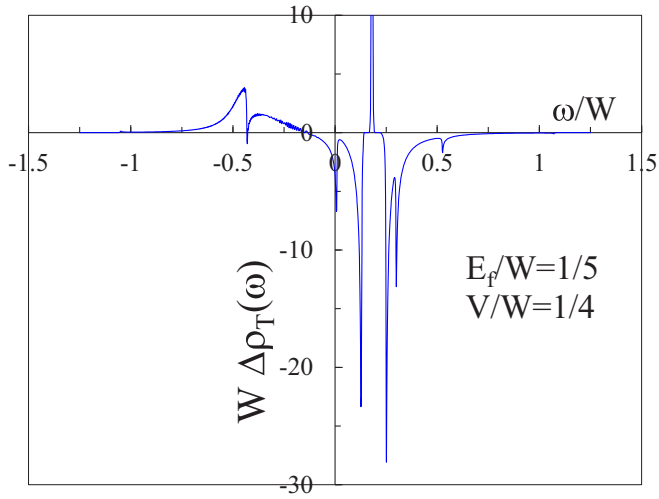

FIG. 2. The change in the total density of states $\Delta\rho_T(\omega)$ due to the presence of the impurity potential. The change in the density of states is shown for the same choice of parameters used in Fig. 1. The value of ΔU was chosen as $-W/2$. It is seen that impurity potential removed spectral weight from the edges of the hybridization gap and formed an in-gap impurity state of weight unity [as is described by Eq. (34)]. The ω-integrated total spectral weight $(2N\sum_\alpha D_\alpha)$ is conserved. The in-gap state has the form of a delta function. Although ΔU is not sufficiently strong to produce a bound state below the lower hybridized band, it is seen that the impurity potential has moved spectral weight of the lower hybridized band to lower energies, thereby forming a virtual bound state with a Fano antiresonance.

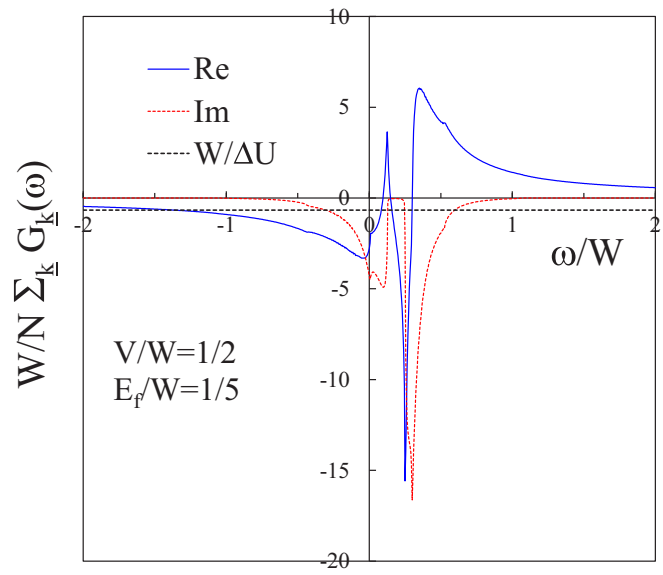

FIG. 3. A plot of the real (blue) and imaginary part (red) of the $\underline{k}$-averaged homogeneous f-electron Green's function $G^{f,0}_{\underline{k}}(\omega)$, in units of the inverse d-bandwidth W^{-1}. The values of E_f/W and V/W were chosen, respectively, as $1/5$ and $1/2$. Bound states occur at energies where $(\frac{1}{\Delta U})$ shown by the horizontal dashed black line intersects with the blue line whenever the imaginary part (shown in red) is zero.

The above expression for the density of states involves the real and imaginary parts of the unperturbed ff-electron Green's function

$$\frac{1}{N}\sum_{\underline{k}} \mathrm{Re}\, eG^{f,0}_{\underline{k},\alpha}(\omega) = \frac{1}{\omega - E_{f,\alpha}} + \frac{|V|^2}{(\omega - E_{f,\alpha})^2} \times \int_{-\infty}^{\infty} d\epsilon \frac{\rho_{0,d}(\epsilon)}{\omega - \frac{|V|^2}{\omega - E_{f,\alpha}} - \epsilon} \quad (29)$$

and

$$\lim_{\eta\to 0}\frac{1}{N}\sum_{\underline{k}} \mathrm{Im}\, mG^{f,0}_{\underline{k},\alpha}(\omega + i\eta) = -\frac{|V|^2}{(\omega - E_{f,\alpha})^2}\pi\rho_{0,d} \times\left(\omega - \frac{|V|^2}{(\omega - E_{f,\alpha})}\right) \quad (30)$$

and their derivatives. The unhybridized d-electron density of states $\rho_{0,d}(\epsilon)$ is nonzero in the energy width $W > \epsilon > -W$. However, the nonmonotonic variation of the argument $\epsilon = \omega - \frac{|V|^2}{\omega - E_{f,\alpha}}$ with ω also forces the imaginary part, shown in Eq. (30), to fall to zero within a hybridization gap of full width

$$\Delta = 2\,\frac{|V|^2}{W} \quad (31)$$

located around $E_{f,\alpha}$. The real and imaginary parts of the unperturbed ff Green's function are sketched in Fig. 3. One sees that the imaginary part (shown in red) has a continuous spectrum which becomes an infinitesimal constant outside the f bandwidth and within the hybridization gap. Bound states may be formed in these energy windows.

Within the hybridization gap at $\omega = E_{f,\alpha}$,

$$\frac{1}{N}\sum_{\underline{k}} \mathrm{Im}\, mG^{f,0}_{\underline{k},\alpha}(\omega + i\eta) \sim -\frac{\eta}{N}\sum_{\underline{k}} \frac{|V|^2 + [E_{f,\alpha} - \epsilon(\underline{k})]^2}{|V|^4}, \quad (32)$$

so the imaginary parts of the unperturbed ff Green's functions are infinitesimal and their derivatives are zero. One may reach this same conclusion by means of an alternate argument. Note that the imaginary part of the ff Green's function can be generated by the replacement $\omega \to \omega + i\eta$ in the purely real part of the Green's function $f(\omega)$, which is analytic and smoothly varying within the hybridization gap. To first order in η, one may Taylor expand

$$f(\omega + i\eta) = f(\omega) + i\eta\frac{\partial f(\omega)}{\partial\omega} + \cdots. \quad (33)$$

As seen in Fig. 3, the function is approximately linear, therefore, one expects that the derivative of $f(\omega)$ will not only be infinitesimal but also approximately constant. Thus, the derivative of the imaginary part of the ff Green's function is expected to be negligibly small. Both arguments imply that, for the energies for which the host's hybridized density of states is zero, the impurity contribution to the density of states is given solely by the second term of Eq. (28) which reduces

to

$$\Delta\rho_T(\omega) = -\frac{\Delta U}{N}\sum_{\underline{k},\alpha}\frac{\partial}{\partial\omega}\mathrm{Re}\, eG^{f,0}_{\underline{k},\alpha}(\omega)\delta \times\left(1-\frac{\Delta U}{N}\sum_{\underline{k}''}\mathrm{Re}\, eG^{f,0}_{\underline{k}'',\alpha}(\omega)\right). \quad (34)$$

Likewise, for ω equal to $E_{f,\alpha}$, one finds that

$$\frac{1}{N}\sum_{\underline{k}}\mathrm{Re}\, eG^{f,0}_{\underline{k},\alpha}(\omega+i\eta)\sim -\frac{\omega-\int d\epsilon\rho_{0,d}(\epsilon)\epsilon}{|V|^2}, \quad (35)$$

where the contributions from the simple poles at $\omega = E_{f,\alpha}$ have canceled. Therefore, due to the small magnitude of the hybridization gap and the asymmetry in the electron density of states, the real part of the ff Green's function is rapidly varying within the hybridization gap. Its slope at $E_{f,\alpha}$ is approximately given by

$$-\frac{1}{N}\sum_{\underline{k}}\frac{\partial}{\partial\omega}\mathrm{Re}\, eG^{f,0}_{\underline{k},\alpha}(\omega)\Big|_{\omega=E_{f,\alpha}}\sim\frac{1}{|V|^2}+\frac{E^2_{f,\alpha}+\int d\epsilon\rho_{0,d}(\epsilon)\epsilon^2}{|V|^4}. \quad (36)$$

As a result, the real part of the $\underline{k}$-averaged unperturbed ff Green's function dips to a very large negative value below the upper edge of the hybridization gap and rises to a very large positive value just above the lower edge of the hybridization gap (as depicted in Fig. 3). Hence, even exceptionally small positive or negative values of ΔU ($|\Delta U| \ll \frac{|V|^2}{E_f}$) are sufficient to produce a solution of the equation

$$\frac{1}{\Delta U} = \frac{1}{N}\sum_{\underline{k}}\mathrm{Re}\, eG^{f,0}_{\underline{k},\alpha}(\omega), \quad (37)$$

thereby producing zeroes in the arguments of delta functions of Eq. (34). The magnitude of the critical value of ΔU can be much smaller than the hybridization gap, which for SmB_6 is of the order of 10–20 meV. Due to band inversion, positive values of ΔU slightly greater than a critical value produce in-gap bound states with energies just above the top of the hybridized valence band, whereas negative values of ΔU produce in-gap bound states just below the top of the hybridized conduction band. Since spectral weight is conserved, the spectral weight of the in-gap bound state is primarily removed from the closest edge of the hybridized band structure. For larger magnitudes of ΔU, the in-gap bound states shift away from the edges of the gap and the spectral weight is shifted to the bound state from both the upper and lower edges of the hybridization gap in almost equal proportions, as can be seen in Fig. 2.

In addition to the bound states within the hybridization gap, sufficiently large values of ΔU may also produce bound states either above or below the topmost or lowermost edge of the hybridized bands. The criterion for the production of a deep-energy bound state is approximately given by

$$|\Delta U| > W. \quad (38)$$

The critical value of ΔU for the second type of states is expected to be of the order of eV, in contrast to the small critical value required to produce in-gap bound states. The spectral weight associated with the formation of the bound states is removed from the continuous portion of the spectrum, and can be expressed in terms of the phase shifts through Levinson's theorem [60]. Positive values of ΔU that are greater than the critical value produce bound states with energies above the top of the conduction band, whereas negative values produce bound states with energies below the bottom of the valence band (as shown in Fig. 4).

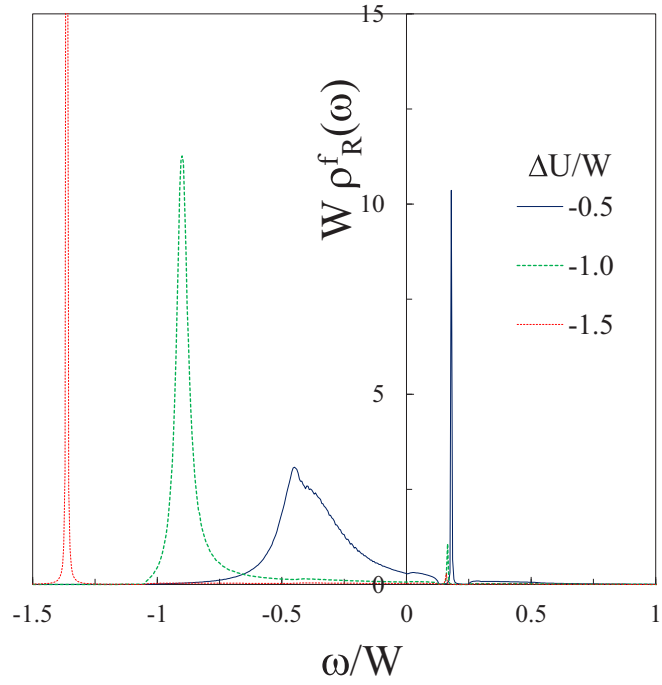

FIG. 4. The energy dependence of the local f-density of states on the impurity site $\rho^f_{\underline{R}=0}(\omega)$ for three values of ΔU, $\Delta U = -1.5W$ (red), $\Delta U = -1.0W$ (green), and $\Delta U = -0.5W$ (blue). The values of E_f and V are the same as in Fig. 2. For all values of ΔU, there is a bound state within the hybridization gap. The delta function has been given a small width to make it visible. It is seen that the intensity of the in-gap bound state is very small and decreases as ΔU^{-2} when ΔU increases. For $\Delta U = -1.5W$, a bound state has split off from the bottom of the band and has removed almost all of the spectral weight from the continuous spectra. For $\Delta U = -0.5W$, an external bound state has not formed, but the on-site impurity potential has shifted spectral weight towards the bottom of the f band producing a virtual bound state.

B. The local density of states

The number of f electrons at the site $\underline{R}$ can be expressed as

$$\langle f^\dagger_{\underline{R},\alpha} f_{\underline{R},\alpha}\rangle = \frac{1}{N}\sum_{\underline{k},\underline{k}'}\exp[i(\underline{k}-\underline{k}')\cdot\underline{R}]\langle f^\dagger_{\underline{k},\alpha}\, f_{\underline{k}',\alpha}\rangle. \quad (39)$$

From which one finds that the f-density of states at site $\underline{R}$ is given by the $\eta\to 0$ limit

$$\rho^f_{\underline{R}}(\omega) = -\frac{1}{\pi}\frac{1}{N}\sum_{\underline{k},\underline{k}',\alpha}\exp[i(\underline{k}-\underline{k}')\cdot\underline{R}]\mathrm{Im}\, mG^{ff}_{\underline{k},\alpha;\underline{k}',\alpha}(\omega+i\eta). \quad (40)$$

The d-density of states at site $\underline{R}$ is given by the analogous limit

$$\rho^d_{\underline{R}}(\omega) = -\frac{1}{\pi}\frac{1}{N}\sum_{\underline{k},\underline{k}',\alpha} \exp[i(\underline{k}-\underline{k}')\cdot\underline{R}]\mathrm{Im}\, m G^{dd}_{\underline{k},\alpha;\underline{k}',\alpha}(\omega+i\eta). \tag{41}$$

On using the expressions for the ff and dd Green's functions, one finds

$$\rho^f_{\underline{R}}(\omega) = -\frac{1}{\pi}\mathrm{Im}\, m\sum_\alpha\left[\frac{1}{N}\sum_{\underline{k},\alpha} G^{f,0}_{\underline{k},\alpha}(\omega) + \frac{1}{N}\sum_{\underline{k}}\exp[i\underline{k}\cdot\underline{R}]G^{f,0}_{\underline{k},\alpha}(\omega)T_\alpha(\omega) \times\frac{1}{N}\sum_{\underline{k}'}\exp[-i\underline{k}'\cdot\underline{R}]G^{f,0}_{\underline{k}',\alpha}(\omega)\right] \tag{42}$$

and

$$\rho^d_{\underline{R}}(\omega) = -\frac{1}{\pi}\mathrm{Im}\, m\sum_\alpha\left[\frac{1}{N}\sum_{\underline{k},\alpha} G^{d,0}_{\underline{k},\alpha}(\omega) + \frac{1}{N}\sum_{\underline{k}}\exp[i\underline{k}\cdot\underline{R}]G^{fd,0}_{\underline{k},\alpha}(\omega)^* T_\alpha(\omega) \times\frac{1}{N}\sum_{\underline{k}'}\exp[-i\underline{k}'\cdot\underline{R}]G^{fd,0}_{\underline{k}',\alpha}(\omega)\right]. \tag{43}$$

1. The local f-density of states

The expression for the f-density of states at the impurity site $\underline{R}=0$ can be simplified, since the phase factors in the term proportional to the T matrix reduce to unity. On using the expression for T matrix, and putting the first and second term over the denominator of the T matrix, one finds that the terms in the numerator proportional to ΔU cancel. Due to the cancellation, the f-density of states at the impurity site $\rho^f_{R=0}(\omega)$ reduces to

$$\rho^f_{R=0}(\omega) = -\frac{1}{\pi}\sum_\alpha \mathrm{Im}\, m\left(\frac{\frac{1}{N}\sum_{\underline{k}} G^{f,0}_{\underline{k},\alpha}(\omega)}{1-\Delta U\frac{1}{N}\sum_{\underline{k}''} G^{f,0}_{\underline{k}'',\alpha}(\omega)}\right) = -\frac{1}{\pi}\sum_\alpha \frac{\frac{1}{N}\sum_{\underline{k}}\mathrm{Im}\, m G^{f,0}_{\underline{k},\alpha}(\omega)}{\left[1-\frac{\Delta U}{N}\sum_{\underline{k}''}\mathrm{Re}\, e G^{f,0}_{\underline{k}'',\alpha}(\omega)\right]^2+\left[\frac{\Delta U}{N}\sum_{\underline{k}''}\mathrm{Im}\, m G^{f,0}_{\underline{k}'',\alpha}(\omega)\right]^2}. \tag{44}$$

Hence, within the hybridization gap, the f-density of states at the impurity site can be simplified as

$$\rho^f_{R=0}(\omega) = \sum_\alpha \frac{1}{\Delta U}\delta\left(1-\frac{\Delta U}{N}\sum_{\underline{k}''}\mathrm{Re}\, e G^{f,0}_{\underline{k}'',\alpha}(\omega)\right), \tag{45}$$

which has an explicit factor of ΔU^{-1}. Therefore, the in-gap bound state has a negligibly small ω-integrated spectral weight on the impurity site which is given by

$$\left[-\Delta U^2\frac{\partial}{\partial\omega}\frac{1}{N}\sum_{\underline{k}''}\mathrm{Re}\, e G^{f,0}_{\underline{k}'',\alpha}(\omega)\right]^{-1} \sim \frac{|V|^4}{W^2\Delta U^2}. \tag{46}$$

The small weight is due to the factor of ΔU^{-1} originating from the cancellation of the phase factors and also a factor involving the derivative that quantifies the wave function or quasiparticle renormalization. Hence, in the limit $\Delta U\to\infty$, the amplitude of the bound state at the impurity site vanishes, in accord with the findings of Sollie and Schlottmann. The f-density of states at the impurity site is shown in Fig. 4 for negative values of ΔU. In addition to the in-gap bound state, spectral weight from the continuum is seen to be shifted to lower energies. For ΔU with magnitude smaller than W, a virtual bound state [61–63] is seen to form at $\omega\sim E_f+\Delta U$ with a width given by $\pi\ V^2\rho_{0,d}(\omega)$ which, as $|\Delta U|$ is increased, moves to lower energies, sharpens up, and then splits off the bottom of the valence band forming a deep energy bound state.

The f-density of states on the nearest neighbor site $\underline{R}=(1,0,0)$ is shown in Fig. 5. As the energy of the bound state approaches E_f, the spectral weight increases towards a maximum value estimated as

$$\frac{\frac{W^2}{36}}{V^2+E_f^2+\frac{W^2}{6}}. \tag{47}$$

Hence, in the wide-band limit, $\frac{1}{6}$ of the in-gap bound state spectral weight is of f character which is equally distributed on the shell of nearest neighboring atoms, in accord with the calculations of Sollie and Schlottmann in the particle-hole symmetric case where $E_f=0$ and $\Delta U\to\infty$. It is seen that the spectral weight in the continuous portion of the $\underline{R}=(1,0,0)$ spectrum is larger than for $\underline{R}=0$. Furthermore, as seen in Fig. 6, there is little change in $\rho^f_{(1,0,0)}(\omega)$ at the bottom of the valence band, even when the deep energy bound state forms. This indicates that both the virtual bound state and the deep-energy bound states are well localized on the scale of a lattice spacing. For $\underline{R}=(2,0,0)$, the f spectrum is almost indistinguishable from the bulk f-density of states.

2. The local d-density of states

The d-density of states at the site of the impurity $\underline{R} = 0$ is given by the expression

$$\rho^{d}_{R=0}(\omega) = -\frac{1}{\pi}\sum_{\alpha} \mathrm{Im}\, m\left(\frac{\left(1-\frac{\Delta U}{\omega - E_{f,\alpha}}\right)\frac{1}{N}\sum_{\underline{k}} G^{d,0}_{\underline{k},\alpha}(\omega)}{1-\Delta U\frac{1}{N}\sum_{\underline{k}''} G^{f,0}_{\underline{k}'',\alpha}(\omega)}\right)$$
$$= -\frac{1}{\pi}\sum_{\alpha}\frac{\mathrm{Re}\, e\left[\left(1-\frac{\Delta U}{\omega - E_{f,\alpha}}\right)\frac{1}{N}\sum_{\underline{k}} G^{d,0}_{\underline{k},\alpha}(\omega)\right]\frac{\Delta U}{N}\sum_{\underline{k}} \mathrm{Im}\, m G^{f,0}_{\underline{k},\alpha}(\omega)}{\left[1-\frac{\Delta U}{N}\sum_{\underline{k}''}\mathrm{Re}\, e G^{f,0}_{\underline{k}'',\alpha}(\omega)\right]^2+\left[\frac{\Delta U}{N}\sum_{\underline{k}''}\mathrm{Im}\, m G^{f,0}_{\underline{k}'',\alpha}(\omega)\right]^2}$$
$$-\frac{1}{\pi}\sum_{\alpha}\frac{\mathrm{Im}\, m\left[\left(1-\frac{\Delta U}{\omega - E_{f,\alpha}}\right)\frac{1}{N}\sum_{\underline{k}} G^{d,0}_{\underline{k},\alpha}(\omega)\right]\left[1-\frac{\Delta U}{N}\sum_{\underline{k}}\mathrm{Re}\, e G^{f,0}_{\underline{k},\alpha}(\omega)\right]}{\left[1-\frac{\Delta U}{N}\sum_{\underline{k}''}\mathrm{Re}\, e G^{f,0}_{\underline{k}'',\alpha}(\omega)\right]^2+\left[\frac{\Delta U}{N}\sum_{\underline{k}''}\mathrm{Im}\, m G^{f,0}_{\underline{k}'',\alpha}(\omega)\right]^2}. \tag{48}$$

The on-site d spectral weight of the in-gap bound state is evaluated to be

$$\frac{V^2}{V^2 + E_f^2 + \frac{W^2}{6}} \tag{49}$$

for moderately small values of ΔU. The sum rule for the in-gap state's spectral weight is saturated by the on-site d and nearest neighbor f weights, in the limit of particle-hole symmetry $E_f \to 0$. As seen in Fig. 7, the continuous portion of the on-site d spectral density exhibits a strong Fano antiresonance [64] at $\omega \sim E_f + \Delta U$. The local d-density of states on the nearest neighbor site $\underline{R} = (1, 0, 0)$ is shown in Fig. 8. When compared with the on-site d-density of states, it is seen that the strength of the antiresonance is diminished on the nearest neighbor sites. The Fano asymmetry parameter $q_{\underline{R}}$ does depend on $\underline{R}$ and varies rapidly with energy but increases when the energy of the virtual bound state decreases towards the bottom of the valence band.

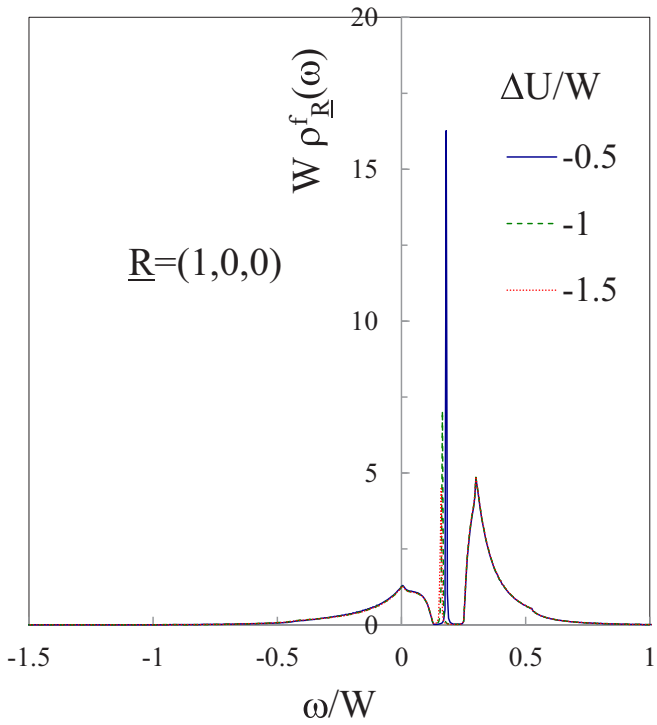

FIG. 5. The local f-density of states on the site $R = (1, 0, 0)$ neighboring the impurity $\rho^{f}_{(1,0,0)}(\omega)$ as a function of ω, for three values of ΔU, $\Delta U = -1.5W$ (red), $\Delta U = -1.0W$ (green), and $\Delta U = -0.5W$ (blue). The values of E_f and V are the same as in Fig. 2. For all values of ΔU, there is a bound state within the hybridization gap. The delta function has been given a small width to make it visible. The intensity of the in-gap bound state on the nearest neighbor site is seen to decrease as the magnitude of ΔU is increased. For $\Delta U = -1.5W$, a bound state has split off from the bottom of the valence band, however, there is no visible vestige of the external bound state on the neighboring site, indicating that it has a localization length less than the lattice spacing.

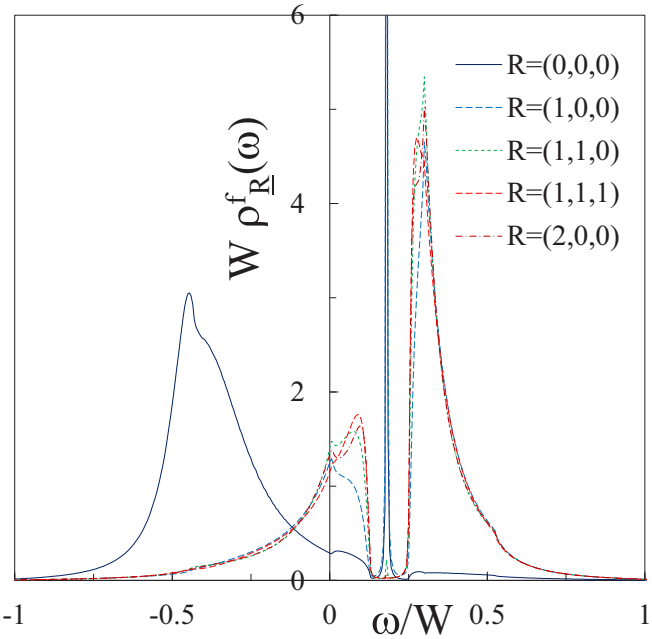

FIG. 6. The energy dependence of the local f-density of states $\rho^{f}_{R}(\omega)$ at site $\underline{R}$ from the impurity, for $\Delta U = -0.5W$. The values of E_f and V are the same as in Fig. 2. For small ΔU, the local f-density of states on the impurity site exhibits a virtual bound state and has a small amplitude of the in-gap bound state. The f weight of the in-gap bound state is primarily located on the sites which are nearest neighbor to the impurity, i.e., $\underline{R} = (1, 0, 0)$. The delta function has been given a small width to make it visible. The amplitude of the in-gap bound decreases with increasing separation from the impurity site.

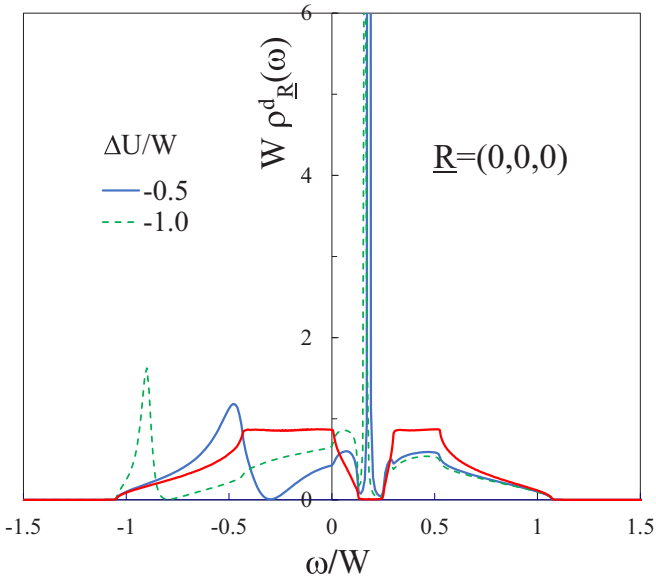

FIG. 7. The local d-density of states on the impurity site $R = (0, 0, 0)$ for $\Delta U = -0.5W$ (blue) and for $\Delta U = -1.0W$ (green) and the bulk d-density of states where $|\underline{R}| \to \infty$ (red). The values of E_f and V are the same as in Fig. 3. There is a bound state on the impurity site within the hybridization gap. The delta function has been given a small width to make it visible. The d-density of states on the impurity site shows a Fano antiresonance near the energy $E_f + \Delta U$ where the f-density of sates exhibits a virtual bound state.

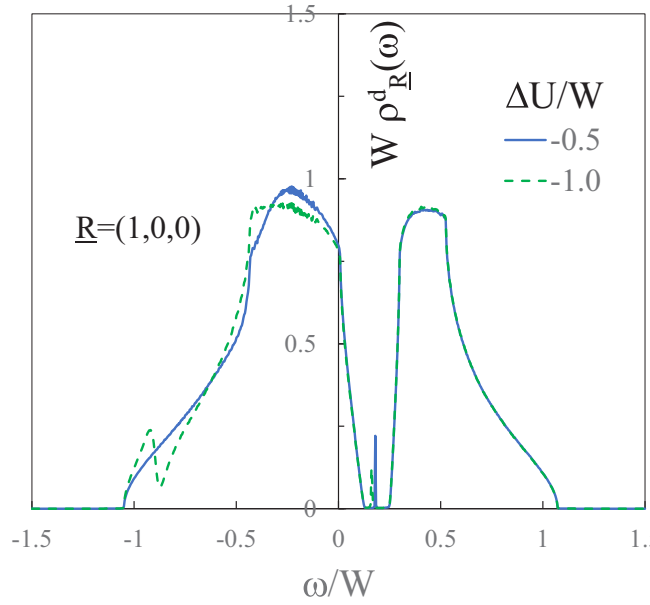

FIG. 8. The energy dependence of the local d-density of states on the site $R = (1, 0, 0)$ neighboring the impurity for $\Delta U = -0.5W$ (blue) and for $\Delta U = -1.0W$ (green). The values of E_f and V are the same as in Fig. 3. The delta function representing the in-gap state has been given a small width to make it visible. A residual small Fano antiresonance occurs on the nearest neighbor site around the energy $E_f + \Delta U$.

IV. SUMMARY

As proposed by Fu, Kane, and Mele [65], an insulator with an odd number of time-reversal invariant (TRI) points in the Brillouin zone is expected to have a nontrivial topology if the parities of the occupied states are reversed at an odd number of TRI points. A continuum of nondegenerate zero-energy surface states is then expected to form at the interface between topologically trivial and topologically nontrivial insulators. As illustrated in Appendix A, this expectation is severely modified if either the topological or nontopological regions have finite spatial extents, in which case, the interface states have finite excitation energies due to the discretization caused by the finite length scale. However, when tunneling across the finite region is suppressed, the lowest excitation energy collapses onto zero. For the half-filled Anderson lattice model, the topological characterization of the insulating state as trivial or nontrivial depends on band inversion [4] since the parities of the TRI points $\underline{k}_m$ are defined by $\delta(\underline{k}_m) = \mathrm{sgn}[\epsilon_\alpha(\underline{k}_m) - E_f]$. If the unperturbed system has a nontrivial topological character, then a uniform relative shift of E_f by $|\Delta U|$ $(<W)$ over a finite region could result in the parities of the occupied states changing. Therefore, an in-gap state may form at the interface between the two regions. For a material with electron-hole symmetry, i.e., $E_f = 0$, the in-gap states are at zero energy, when tunneling across the region is suppressed by a large $|\Delta U|$. Thus, even if the region in which band inversion occurs is restricted to one site, $|\Delta U|$ may suppress tunneling and lead to low-energy surface states that may have nontrivial topologically characters.

We have shown using the hybridization gap model of a Kondo insulator that nonmagnetic impurities may produce two types of bound states. One set of bound states only form if the impurity potential exceeds a critical value which is comparable to the bandwidth. These bound states are split off from the upper (lower) edge of the conduction (valence) band and are related to the bound states found in topologically trivial metals [59]. For values of the impurity potential smaller than the critical value, the states merge with the continuous portions of the density of states and form broadened virtual bound states. The other type of bound states form within the hybridization gap and occur for extremely small values of the impurity potential which can be significantly smaller than the hybridization gap when the density of states is highly asymmetric. This illustrates the extreme sensitivity of Kondo insulators to imperfections. The in-gap bound states gap have the form of surface states that extend over shells neighboring the impurity. In other words, they form metallic states on the surface surrounding the defect, much the same way as the surface of topological insulators supports a metallic surface states which surrounds the insulating bulk. The existence of the hybridization gap and the in-gap states is due to the band inversion present in the model. If the features of the hybridization gap model are adjusted to accommodate the conditions necessary for the classification as a topological insulator [4], the in-gap impurity states are also expected to have nontrivial topological character.

ACKNOWLEDGMENTS

The work at Temple was supported by the US Department of Energy, Office of Basic Energy Science, Materials Science,

through the Award DE-FG02-01ER45872. P.S.R. would like to acknowledge stimulating discussions with Z. Fisk.

APPENDIX A

In this Appendix we consider a model of a topological insulator given by the Dirac equation with a spatially dependent mass [52,53], for two types of geometries. If the mass changes sign at a surface separating two regions, the system remains insulating deep with each region but the parities of the solution in these regions are reversed. Since the Dirac equation only has one trivial time-reversal invariant point, a switch in the mass results in a switch of parity which leads to the interface being classified as one which joins a topological nontrivial and a topological trivial region.

1. TI thin film

A thin film of a topological insulator with an energy gap of $2mc^2$ surrounded by a topologically trivial insulator with the same magnitude of the gap. We assume that the mass depends on the spatial coordinate z via

$$m(z) = m\,(1 - 2\Theta(z+a) + 2\Theta(z-a)). \tag{A1}$$

The Dirac equation has surface states [55] with a dispersion relation given by

$$\left(\frac{E}{c}\right)^2 - (\hbar \underline{k}_{\|})^2 + (m_1 c\,)^2 = (mc)^2, \tag{A2}$$

where $k_{\|}$ is the component of the momentum parallel to the surface and the term proportional to m_1^2 represents the negative kinetic energy due to tunneling. The surface states exponentially decay over a length scale ξ given by

$$\xi = \frac{\hbar}{m_1 c}, \tag{A3}$$

where the decay length is determined by m_1 which is given by the solution of

$$\exp\left[-4\frac{m_1 c}{\hbar}a\right] = 1 - \left(\frac{m_1}{m}\right)^2. \tag{A4}$$

Therefore, in the limit $a \to \infty$, one finds that m_1 increased monotonically $m_1 \to m$ and the dispersion relation for the surface excitations becomes gapless. The monotonic decrease in the magnitude of the gap with increasing a has been observed [56] in photoemission experiments on Bi_2Se_3. In the limit $a \to \infty$, the simultaneous energy $k_{\|}$ eigenstates are twofold degenerate. One choice of basis consists of a pair of surface states, one localized at the front surface and one localized around the back surface of the film. The effective Hamiltonian for the upper components of the surface state Dirac spinor reduces to a Rashba spin-orbit coupling Hamiltonian, therefore, the pair of orthogonal surface states exhibits spin-momentum locking, in which the spins are aligned parallel to the surface with directions perpendicular to the in-plane momenta. However, a linear superposition of the precisely degenerate states leads to charge fractionalization [52] and a net normal component of the thin film's magnetization.

2. Spherical void in a TI

A spherical void in a topological insulator can be described by the Dirac equation, in which the mass $m(r)$ is dependent on the radial distance. The four-component Dirac spinor Ψ can be represented in terms of two two-component spinors

$$\Psi = \frac{1}{r}\begin{pmatrix} f(r)\Omega_{j,j_z}^{j\pm\frac{1}{2}} \\ i\,g(r)\Omega_{j,j_z}^{j\mp\frac{1}{2}} \end{pmatrix} \tag{A5}$$

in which the orbital angular momentum is given by $l = j \pm \frac{1}{2}$ and where the two-component spinor-spherical harmonics are given by

$$\begin{aligned}\Omega_{j,j_z}^{j+\frac{1}{2}} &= -\sqrt{\frac{j+1-j_z}{2j+2}}Y_{j_z-\frac{1}{2}}^{j+\frac{1}{2}}(\theta,\varphi)\begin{pmatrix}1\\0\end{pmatrix} \\ &\quad + \sqrt{\frac{j+1+j_z}{2j+2}}Y_{j_z+\frac{1}{2}}^{j+\frac{1}{2}}(\theta,\varphi)\begin{pmatrix}0\\1\end{pmatrix}, \\ \Omega_{j,j_z}^{j-\frac{1}{2}} &= \sqrt{\frac{j+j_z}{2j}}Y_{j_z-\frac{1}{2}}^{j-\frac{1}{2}}(\theta,\varphi)\begin{pmatrix}1\\0\end{pmatrix} + \sqrt{\frac{j-j_z}{2j}}\,Y_{j_z+\frac{1}{2}}^{j-\frac{1}{2}}(\theta,\varphi)\begin{pmatrix}0\\1\end{pmatrix}.\end{aligned} \tag{A6}$$

It should be noted that the upper and lower components of the energy eigenfunctions of the Dirac equation have different l values and, therefore, have different parities. The spinor spherical harmonics are related by the identity

$$\left(\frac{\underline{\sigma}\cdot\underline{r}}{r}\right)\Omega_{j,j_z}^{j+\frac{1}{2}} = -\Omega_{j,j_z}^{j-\frac{1}{2}}, \tag{A7}$$

in which $\underline{\sigma}$ is the vector spin operator with components given by the Pauli matrices. The radial functions $f(r)$ and $g(r)$ satisfy the set of coupled equations

$$\begin{aligned}[E - U(r) - m(r)c^2]f - c\hbar\left(\frac{\partial}{\partial r} - \frac{\kappa}{r}\right)g = 0, \\ [E - U(r) + m(r)c^2]g + c\hbar\left(\frac{\partial}{\partial r} + \frac{\kappa}{r}\right)f = 0,\end{aligned} \tag{A8}$$

where $\kappa = \pm(j+\frac{1}{2})$ and $U(r)$ is a spatially varying electrostatic potential. Generally, the energy eigenstates of the spherically symmetric Dirac equation are classified by the three quantum numbers (j, j_z, κ). We shall consider the mass to have the form

$$m(r) = M - (M+m)\Theta(r-a), \tag{A9}$$

such that the system is topologically nontrivial in the region where $r > a$ and topologically trivial in the region $r < a$. The spherical boundary at $r = a$ separates the void from the topological insulator [66]. The electrostatic potential is chosen to be nonzero inside the void

$$U(r) = \Delta U\,\Theta(a-r). \tag{A10}$$

Since the mass and the electrostatic potential $U(r)$ are constant in either region, one may define radial quantum numbers for each region by

$$\begin{aligned}(E - \Delta U)^2 - M^2c^4 &= \hbar^2c^2k_<^2, \\ E^2 - m^2c^4 &= \hbar^2c^2k_>^2.\end{aligned} \tag{A11}$$

The bulk states correspond to positive values of k, but the in-gap states are found by analytically continuing k to imaginary values. When expressed in terms of the dimensionless variables $\rho = kr$, one finds that the solutions in the two regions satisfy the Riccatti-Bessel equation. On setting

$$f(\rho) = A\sqrt{\rho}Z_{|\kappa+\frac{1}{2}|},$$
$$g(\rho) = B\sqrt{\rho}Z_{|\kappa-\frac{1}{2}|}, \tag{A12}$$

one finds that the solutions are of the form of Bessel functions of half-integer order. For $r > a$, normalizability requires that the allowed solutions are Bessel functions of the first kind, $Z_{|\kappa\pm\frac{1}{2}|} = J_{|\kappa\pm\frac{1}{2}|}$. The Bessel function recursion relations

$$J_{\nu-1} + J_{\nu+1} = \frac{2\nu}{\rho}J_\nu,$$
$$J_{\nu-1} - J_{\nu+1} = 2\frac{\partial J_\nu}{\partial\rho} \tag{A13}$$

for $\nu > 0$ can be used to yield the relation between the amplitudes of the upper and lower components:

$$\left(\frac{E - \Delta U - Mc^2}{c\hbar k_<}\right)A_< = -\mathrm{sgn}(\kappa)\, B_<, \tag{A14}$$

Since we are interested in the in-gap states, the solutions in the exterior region will be restricted to the Hankel functions $H^{(1)}_{|\kappa\pm\frac{1}{2}|}$ which have an asymptotic variation of

$$H^{(1)}_{|\kappa+\frac{1}{2}|}(\rho) \sim \frac{1}{\sqrt{\rho}}\ \exp[+i\rho], \tag{A15}$$

which are exponentially decaying when $k_>$ is analytically continued to imaginary values. The Bessel function recursion relations lead to the relation between the amplitudes of the upper and lower components

$$\left(\frac{E + mc^2}{c\hbar k_>}\right)A_> = -\mathrm{sgn}(\kappa)\, B_>. \tag{A16}$$

Continuity of the spinorial wave function at $r = a$ leads to the energy eigenvalue equation

$$\left(\frac{E - \Delta U + Mc^2}{c\hbar k_<}\right)\left(\frac{j_{|\kappa+\frac{1}{2}|-\frac{1}{2}}(k_<a)}{j_{|\kappa-\frac{1}{2}|-\frac{1}{2}}(k_<a)}\right)$$
$$= \left(\frac{E - mc^2}{c\hbar k_>}\right)\left(\frac{h^{(1)}_{|\kappa+\frac{1}{2}|-\frac{1}{2}}(k_>a)}{h^{(1)}_{|\kappa-\frac{1}{2}|-\frac{1}{2}}(k_>a)}\right) \tag{A17}$$

expressed in terms of the spherical Bessel functions. Therefore, the eigenstates are degenerate with respect to j_z, so the energy can only depend on j and possibly on the parity $(-1)^{|\kappa+\frac{1}{2}|-\frac{1}{2}}$. The spherical Bessel functions are defined by

$$j_\nu(\rho) = \sqrt{\frac{\pi}{2\rho}}J_{\nu+\frac{1}{2}}(\rho),$$
$$h^{(1)}_\nu(\rho) = \sqrt{\frac{\pi}{2\rho}}\,H^{(1)}_{\nu+\frac{1}{2}}(\rho). \tag{A18}$$

The first few analytic continued spherical Bessel functions are given in Table I.

TABLE I. The first few spherical Bessel functions continued to imaginary arguments.

ν	$j_\nu(ix)$	$h^{(1)}_\nu(ix)$
0	$\frac{\sinh x}{x}$	$-\frac{e^{-x}}{x}$
1	$i(\frac{x\cosh x-\sinh x}{x^2})$	$i\frac{e^{-x}}{x}(\frac{1+x}{x})$
2	$-(\frac{(3+x^2)\sinh x-3x\cosh x}{x^3})$	$\frac{e^{-x}}{x}(\frac{3+3x+x^2}{x^2})$
3	$-i(\frac{(15x+x^3)\cosh x-(15+6x^2)\sinh x}{x^4})$	$-i\frac{e^{-x}}{x}(\frac{15+15x+6x^2+x^3}{x^3})$
4	$(\frac{(105+45x^2+x^4)\sinh x-(105x+10x^3)\cosh x}{x^5})$	$-\frac{e^{-x}}{x}(\frac{105+105x+45x^2+10x^3+x^4}{x^4})$

The in-gap state eigenvalue equation only has positive energy solutions for positive values of κ, $\kappa = (j + \frac{1}{2})$, as expected from the band inversion in a topological insulator. Hence, the surface states can be uniquely characterized by the sign of their energies and (j, j_z). As a result, the surface states have lost half their degrees of freedom, due to the locking of the spin with orbital angular momentum. The bound state energies as a function of the radius a and representative probability distributions for $j = \frac{1}{2}$ are shown in Fig. 9. Note that the surface states have inverted parity.

APPENDIX B

The slave boson Hamiltonian for an inhomogeneous Anderson lattice model in the mean-field approximation is expressed as

$$\hat{H}_{\mathrm{MF}} = \sum_{i,\sigma}(E_{f,i} + \lambda_i)f^\dagger_{i,\sigma}f_{i,\sigma} + \sum_{\underline{k},\sigma}\epsilon_{\underline{k}}d^\dagger_{\underline{k},\sigma}d_{\underline{k},\sigma} + \sum_i \lambda_i\, b^*_i b_i$$
$$+ \frac{1}{\sqrt{N}}\sum_{i,\underline{k}.\sigma}[e^{i\underline{k}\cdot\underline{R}_i}V(\underline{k})f^\dagger_{i,\sigma}d_{\underline{k},\sigma}b_i$$
$$+ e^{-i\underline{k}\cdot\underline{R}_i}V^*(\underline{k})b^*_i d^\dagger_{\underline{k},\sigma}f_{i,\sigma}]. \tag{B1}$$

The impurity is modeled by a shift of the f binding energy on site $\underline{R}_0 = 0$ from its uniform value E_f by ΔU,

$$E_{f,i} = E_f + \Delta U\ \delta_{i,0}. \tag{B2}$$

For a paramagnetic phase, the complex slave boson fields b_i satisfies the constraints

$$b^*_i b_i = 1 - D_\alpha\sum_i\langle f^\dagger_i f_i\rangle, \tag{B3}$$

which projects out multiple occupancy on site $\underline{R}_i$ and the Lagrange undetermined parameters λ_i satisfy the extremal condition

$$\lambda_i b^*_i + \frac{D_\alpha}{\sqrt{N}}\sum_{\underline{k}} e^{i\underline{k}\cdot\underline{R}_i}V(\underline{k})\langle f^\dagger_i d_{\underline{k}}\rangle = 0, \tag{B4}$$

where the factor of D_α accounts for the spin degeneracy. The impurity induces a deviation of the boson condensate, which is mainly centered on the impurity ion and almost completely recovers on the sites nearest to the impurity [58]. Therefore, we shall write

$$b_i = b + \Delta b\delta_{i,0},$$
$$\lambda_i = \lambda + \Delta\lambda\delta_{i,0}. \tag{B5}$$

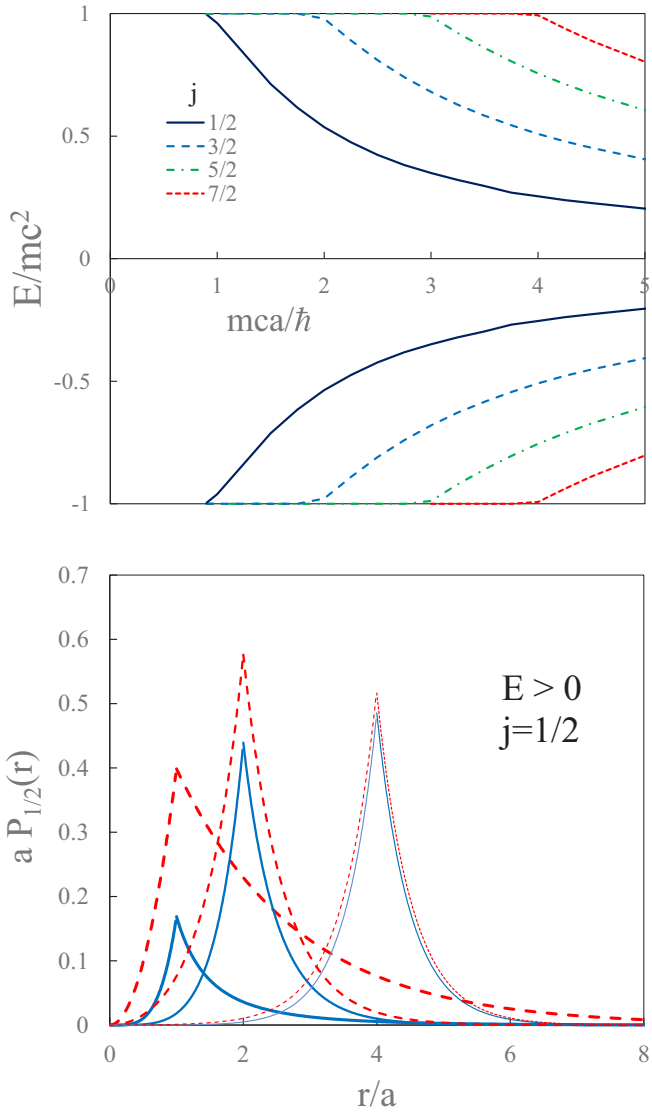

FIG. 9. (Top panel) The bound state energies for $j = \frac{1}{2}$, $j = \frac{3}{2}$, $j = \frac{5}{2}$, ... as a function of the ratio of the radius a to the decay length $\frac{\hbar}{mc}$. (Bottom panel) The radial distribution functions for the upper components ($l = 1$ solid blue) and lower components ($l = 0$ dashed red) of the $j = \frac{1}{2}$ positive energy bound state for $a = 1$ (thick), $a = 2$ (medium), and $a = 4$ (fine).

The following analysis has been extended to deviations of the boson amplitudes which extend to the nearest neighbor sites.

1. Green's functions

The self-consistency equations can be found by solving the inhomogeneous mean-field equations of motion for the f-f and d-f Green's functions. The momentum-dependent f-f Green's function is found as

$$G^{ff}_{\underline{k},\underline{k}'}(\omega) = \mathcal{G}^{ff}{}_{\underline{k}}(\omega)\,\delta_{\underline{k},\underline{k}'} + \mathcal{G}^{ff}{}_{\underline{k}}(\omega)\,T_{\underline{k},\underline{k}'}(\omega)\mathcal{G}^{ff}{}_{\underline{k}'}(\omega), \quad \text{(B6)}$$

where $\mathcal{G}^{ff}{}_{\underline{k}}(\omega)$ is the homogeneous Green's function given by

$$\mathcal{G}^{ff}{}_{\underline{k}}(\omega) = \frac{(\hbar\omega - \epsilon_{\underline{k}})}{(\hbar\omega - E_f - \lambda)(\hbar\omega - \epsilon_{\underline{k}}) - |bV(\underline{k})|^2}, \quad \text{(B7)}$$

and $T_{\underline{k},\underline{k}'}(\omega)$ is the T matrix. The T matrix can be expressed as

$$T_{\underline{k},\underline{k}'}(\omega) = \frac{1}{N}\left(\frac{A^0 + A^1(\underline{k},\underline{k}') + A^2(\underline{k},\underline{k}')}{\Delta(\omega)}\right), \quad \text{(B8)}$$

where the terms in the numerator are expressed as

$$A^0 = \Delta U + \Delta\lambda + \frac{1}{N}\sum_{\underline{k}_1}\Lambda(\underline{k}_1)|\Delta b|^2,$$

$$A^1(\underline{k},\underline{k}') = \Lambda(\underline{k})b\Delta b^* + \Delta b b^*\Lambda(\underline{k}'),$$

$$A^2(\underline{k},\underline{k}') = |\Delta b|^2|b|^2\frac{1}{N}\sum_{\underline{k}_1}\mathcal{G}^{ff}{}_{\underline{k}_1}(\omega)[\Lambda(\underline{k}_1) - \Lambda(\underline{k})] \times [\Lambda(\underline{k}_1) - \Lambda(\underline{k}')], \quad \text{(B9)}$$

and where the denominator $\Delta(\omega)$ is given by

$$\Delta(\omega) = 1 - B^1 - B^2, \quad \text{(B10)}$$

where the terms are

$$B^1 = \frac{1}{N}\sum_{\underline{k}_1}\mathcal{G}^{ff}{}_{\underline{k}_1}(\omega)[A^0 + \Lambda(\underline{k}_1)(b\Delta b^* + b^*\Delta b)],$$

$$B^2 = |\Delta b|^2|b|^2\frac{1}{2N^2}\sum_{\underline{k}_1,\underline{k}_2}\mathcal{G}^{ff}{}_{\underline{k}_1}(\omega)\mathcal{G}^{ff}{}_{\underline{k}_2}(\omega)[\Lambda(\underline{k}_1) - \Lambda(\underline{k}_2)]^2, \quad \text{(B11)}$$

in which

$$\Lambda(\underline{k}) = \frac{|V(\underline{k})|^2}{(\hbar\omega - \epsilon_{\underline{k}})}. \quad \text{(B12)}$$

Despite the fact that the denominator depends on products of spectral functions, due to cancellations Im $m\ \Delta(\omega)$ is zero for frequencies outside the continua of the homogeneous host. As seen in Fig. 10, the poles in the T matrix found using slave boson mean-field calculations are in a one-to-one correspondence with those of the noninteracting model described in the main text.

The d-f Green's function is obtained by the same analysis and is given by

$$G^{df}_{\underline{k},\underline{k}'}(\omega) = \left(\delta_{\underline{k},\underline{k}'}b^* + \frac{\Delta b^*}{N\Delta(\omega)}\right)\mathcal{G}^{df}{}_{\underline{k}}(\omega) + \mathcal{G}^{df}{}_{\underline{k}}(\omega)b^*S_{\underline{k}'}(\omega)\mathcal{G}^{ff}{}_{\underline{k}'}(\omega), \quad \text{(B13)}$$

where the homogeneous d-f Green's function is given by

$$\mathcal{G}^{df}{}_{\underline{k}}(\omega) = \frac{V^*(\underline{k})}{(\hbar\omega - E_f - \lambda)(\hbar\omega - \epsilon_{\underline{k}}) - |bV(\underline{k})|^2} \quad \text{(B14)}$$

and $S_{\underline{k}'}(\omega)$ is given by

$$S_{\underline{k}'}(\omega) = \left(\frac{\Delta U + \Delta\lambda + [\Delta b^* b + b^*\Delta b + |\Delta b|^2]\Lambda(\underline{k}')}{N\Delta(\omega)}\right). \quad \text{(B15)}$$

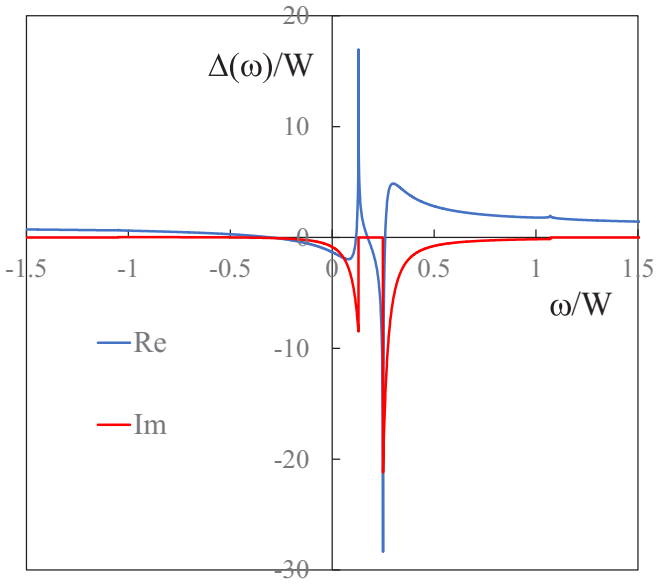

FIG. 10. The ω dependence of the real and imaginary parts of the denominator of the T matrix $\Delta(\omega)$ in dimensionless units. For the chosen parameters, the T matrix has a pole at an energy inside the hybridization gap and a pole at the energy of a virtual bound state.

For the case of a uniform Bose condensate, these results reduce to those given in the main text.

2. Inhomogeneous self-consistency conditions

The f occupation of the central site $\underline{R} = 0$ is given by

$$n_f(\underline{R}=0) = -\frac{D_\alpha}{N}\sum_{\underline{k},\underline{k}'}\int_{-\infty}^{\infty}\frac{d\omega}{\pi}f(\omega)\mathrm{Im}\,m G^{ff}_{\underline{k},\underline{k}'}(\omega)$$
$$= -\frac{D_\alpha}{N}\sum_{\underline{k}}\int_{-\infty}^{\infty}\frac{d\omega}{\pi}f(\omega)\mathrm{Im}\,m\left[\frac{\mathcal{G}^{ff}_{\underline{k}}(\omega)}{\Delta(\omega)}\right], \tag{B20}$$

which is related to the slave boson amplitude at the impurity site $(b^* + \Delta b^*)$. Likewise, the Lagrange parameter at the origin is found from the equation

$$(\lambda + \Delta\lambda)(b^* + \Delta b^*) = -\frac{D_\alpha}{N}\sum_{\underline{k}_1,\underline{k}_2} V(\underline{k}_1)\langle f^\dagger_{\underline{k}_2}\, d_{\underline{k}_1}\rangle. \tag{B21}$$

That inhomogeneous part can be evaluated as

$$(\lambda + \Delta\lambda)(b^* + \Delta b^*) - \lambda b^*$$
$$= -D_\alpha\int_{-\infty}^{\infty}\frac{d\omega}{\pi}f(\omega)\mathrm{Im}\,m\left[\frac{C(\omega)}{\Delta(\omega)}\frac{1}{N}\sum_{\underline{k}_1}\Lambda(\underline{k}_1)\mathcal{G}^{ff}_{\underline{k}_1}(\omega)\right], \tag{B22}$$

Finally, the d-d Green's function is expressed as

$$G^{dd}_{\underline{k},\underline{k}'}(\omega) = \delta_{\underline{k},\underline{k}'}\mathcal{G}^{dd}{}_{\underline{k}}(\omega) + \mathcal{G}^{df}{}_{\underline{k}}(\omega)R(\omega)\mathcal{G}^{fd}{}_{\underline{k}'}(\omega), \tag{B16}$$

where $R(\omega)$ is found as

$$R(\omega) = \left(\frac{|b|^2\Delta U + (\hbar\omega - E_f - \lambda)[\Delta b b^* + b\Delta b^* + |\Delta b|^2]}{N\,\Delta(\omega)}\right). \tag{B17}$$

Or, equivalently

$$G^{dd}_{\underline{k},\underline{k}'}(\omega) = \delta_{\underline{k},\underline{k}'}\mathcal{G}^{dd}{}_{\underline{k}}(\omega) + \mathcal{G}^{df}{}_{\underline{k}}(\omega)P(\omega)\mathcal{G}^{fd}{}_{\underline{k}'}(\omega)$$
$$+\frac{V^*(\underline{k})}{\hbar\omega - \epsilon(\underline{k})}\left(\frac{\Delta b^* b + \frac{1}{2}|\Delta b|^2}{N\,\Delta(\omega)}\right)\mathcal{G}^{fd}_{\underline{k}'}(\omega)$$
$$+\mathcal{G}^{df}_{\underline{k}}(\omega)\left(\frac{b^*\Delta b + \frac{1}{2}|\Delta b|^2}{N\Delta(\omega)}\right)\frac{V(\underline{k}')}{\hbar\omega - \epsilon(\underline{k}')}, \tag{B18}$$

where $P(\omega)$ is given by

$$P(\omega) = |b|^2\left(\frac{\Lambda(\underline{k})\left[\Delta b^* b + \frac{1}{2}|\Delta b|^2\right] + \Delta U + \Delta\lambda + \left[b^*\Delta b + \frac{1}{2}|\Delta b|^2\right]\Lambda(\underline{k}')}{N\Delta(\omega)}\right). \tag{B19}$$

where

$$C(\omega) = \Delta b^* + \frac{b^*}{N}\sum_{\underline{k}_2}\left[(\Delta U + \Delta\lambda)\mathcal{G}^{ff}_{\underline{k}_2}(\omega) + (\Delta b b^*\right.$$
$$\left. + \Delta b^* b + |\Delta b|^2)\Lambda(\underline{k}_2)\mathcal{G}^{ff}_{\underline{k}_2}(\omega)\right]. \tag{B23}$$

Similar to the bulk self-consistency equations, when the energy of the f-impurity state $E_f + \Delta U$ is far below the gap, the constraint λ leads to a large upward shift of the effective impurity level towards the Fermi energy and leads to a further reduction of the weight of the local quasiparticle density of states. This result is analogous to the Kondo limit of an impurity model in a metal, in which the width of the Abrikosov-Suhl resonance above just above the Fermi energy depends exponentially on the separation between the bare f level and the Fermi energy. Our result is also in accord with the results of Alexandrov *et al.* [58], who found that the $T = 0$ solutions of the mean-field slave boson consistency equations remain nontrivial in the presence of inhomogeneity.

The results obtained from our mean-field slave boson calculations are in accord with those described in the main text. The main difference is that, when the bare impurity level lies outside the gap, the on-site f quasiparticle weight is finite but exponentially small, which leads to the incoherent peak at $(E_f + \Delta U)$ having the dominant on-site spectral weight. However, although the poles of the T matrix show the presence of both an in-gap bound state and the deep-energy bound

state, the local f density of states

$$\rho^{f}_{\underline{R}=0}(\omega) = -\frac{1}{\pi}\sum_{\underline{k},\alpha} \mathrm{Im}\, m\left[\frac{\mathcal{G}^{ff}_{\underline{k}}(\omega)}{N\Delta(\omega)}\right] \tag{B24}$$

shows no spectral weight at the in-gap pole. This is due to the entire f spectral weight of the in-gap f state being distributed on the nearest neighbor atoms, as is discussed in the main text.

[1] G. Aeppli and Z. Fisk, Kondo insulators, Comm. Condens. Matter Phys. **16**, 155 (1992).

[2] P. S. Riseborough, Heavy fermion semiconductors, Adv. Phys. **49**, 257 (2000).

[3] P. S. Riseborough, Theory of the dynamic magnetic response of $Ce_3Bi_4Pt_3$—A heavy-fermion semiconductor, Phys. Rev. B **45**, 13984 (1992).

[4] M. Dzero, K. Sun, V. Galitski, and P. Coleman, Topological Kondo Insulators, Phys. Rev. Lett. **104**, 106408 (2010).

[5] T. Takimoto, SmB_6: A promising candidate for a topological insulator, J. Phys. Soc. Jpn. **80**, 123710 (2011).

[6] A. P. Schnyder, S. Ryu, A. Furusaki, and A. W. W. Ludwig, Classification of topological insulators and superconductors in three spatial dimensions, Phys. Rev. B **78**, 195125 (2008).

[7] A. Menth, E. Buehler, and T. H. Geballe, Magnetic and Semiconducting Properties of SmB_6, Phys. Rev. Lett. **22**, 295 (1969).

[8] J. C. Nickerson, R. M. White, K. N. Lee, R. Bachmann, T. H. Geballe, and G. W. Hull, Physical properties of SmB_6, Phys. Rev. B **3**, 2030 (1971).

[9] J. W. Allen, B. Batlogg, and P. Wachter, Large low-temperature Hall effect and resistivity in mixed valent SmB_6, Phys. Rev. B **20**, 4807 (1979).

[10] S. Wolgast, C. Kurdak, K. Sun, J. W. Allen, D.-J. Kim, and Z. Fisk, Low-temperature surface conduction in the Kondo insulator SmB_6, Phys. Rev. B **88**, 180405(R) (2013).

[11] D.-J. Kim, S. Thomas, T. Grant, J. Botimer, Z. Fisk, and J. Xia, Surface Hall effect and nonlocal transport in SmB_6: Evidence for surface conduction, Sci. Rep. **3**, 3150 (2013).

[12] D.-J. Kim, J. Xia, and Z. Fisk, Topological surface state in the Kondo insulator samarium-hexaboride, Nat. Mater. **13**, 466 (2014).

[13] P. Syers, D. Kim, M. S. Fuhrer, and J. Paglione, Tuning Bulk and Surface Conduction in the Proposed Topological Kondo Insulator SmB_6, Phys. Rev. Lett. **114**, 096601 (2015).

[14] Y.-S. Eo, K. Sun, C. Kurdak, D.-J. Kim, and Z. Fisk, Inverted Resistance Measurements as a Method for Characterizing the Bulk and Surface Conductivities of Three-Dimensional Topological Insulators, Phys. Rev. Appl. **9**, 044006 (2018).

[15] Y. S. Eo, A. Rakoski, J. Lucien, D. Mihaliov, Ç. Kurdak, P. F. S. Rosa, D.-J. Kim, and Z. Fisk, Transport gap in SmB_6 protected against disorder, PNAS **116**, 12638 (2019).

[16] M. Neupane, N. Alidoust, S.-Y. Xu, T. Kondo, Y. Ishida, D. J. Kim, C. Liu, I. Belopolski, Y. J. Cho, T. R. Chang, T. Durakiewicz, L. Balicas, H. Lin, A. Bansil, S. Shin, Z. Fisk, and M. Z. Hasan, Surface electronic structure of the topological Kondo-insulator candidate correlated electron system SmB_6, Nat. Commun. **4**, 2991 (2013).

[17] J. Jiang, S. Li, T. Zhang, Z. Sun, F. Chen, Z. R. Ye, M. Xu, Q. Q. Ge, S. Y. Tan, X. H. Niu, M. Xia, B. P. Xie, Y. F. Li, X. H. Chen, H. H. Wen, and D. L. Feng, Observation of possible topological in-gap surface states in the Kondo insulator SmB_6 by photoemission, Nat. Commun. **4**, 3010 (2013).

[18] N. Xu, X. Shi, P. K. Biswas, C. E. Matt, R. S. Dhaka, Y. Huang, N. C. Plumb, M. Radovic, J. H. Dil, E. Pomjakushina, K. Conder, A. Amato, Z. Salman, D. McK. Paul, J. Mesot, H. Ding, and M. Shi, Surface and bulk electronic structure of the strongly correlated system SmB_6 and implications for a topological Kondo insulator, Phys. Rev. B **88**, 121102(R) (2013).

[19] W. Ruan, C. Ye, M. Guo, F. Chen, X. Chen, G.-M. Zhang, and Y. Wang, Emergence of a Coherent In-Gap State in the SmB_6 Kondo Insulator Revealed by Scanning Tunneling Spectroscopy, Phys. Rev. Lett. **112**, 136401 (2014).

[20] S. Roessler, T.-H. Jang, D.-J. Kim, L. H. Tjeng, Z. Fisk, F. Steglich, and S. Wirth, Hybridization gap and Fano resonance in SmB_6, Proc. Natl. Acad. Sci. **111**, 4798 (2014).

[21] W.-K. Park, L. Sun, A. Noddings, D.-J. Kim. Z. Fisk, and L. H. Greene, Topological surface states interacting with bulk excitations in the Kondo insulator SmB_6 revealed via planar tunneling spectroscopy, Proc. Natl. Acad. Sci. **113**, 6599 (2016).

[22] J. Jiao, S. Roessler, D.-J. Kim, L. H. Tjeng, Z. Fisk, F. Steglich, and S. Wirth, Additional energy scale in SmB_6 at low-temperature, Nat. Commun. **7**, 13762 (2016).

[23] L. Sun, D.-J. Kim, Z. Fisk, and W. K. Park, Planar tunneling spectroscopy of the topological Kondo insulator SmB_6, Phys. Rev. B **95**, 195129 (2017).

[24] T. Miyamachi, S. Suga, M. Ellguth, C. Tusche, C. M. Schneider, F. Iga, and F. Komori, Evidence for in-gap surface states on single phase SmB_6 (001) surfaces, Sci. Rep. **7**, 12837 (2017).

[25] P. A. Alekseev, J.-M. Mignot, J. Rossatmignod, V. N. Lazukov, and I. P. Sadikov, Magnetic excitations in SmB_6 single crystals, Physica B Condens. Matter **186-188**, 384 (1993).

[26] W. T. Fuhrman, J. Leiner, P. Nikolic, G. E. Granroth, M. B. Stone, M. D. Lumsden, L. DeBeer-Schmitt, P. A. Alekseev, J.-M. Mignot, S. M. Koohpayeh, P. Cottingham, W. A. Phelan, L. Schoop, T. M. McQueen, and C. Broholm, Interaction Driven Subgap Spin-Exciton in the Kondo Insulator SmB_6, Phys. Rev. Lett. **114**, 036401 (2015).

[27] P. S. Riseborough, Magnetic bound states in SmB_6, Ann. Phys. **9**, 813 (2000); Spin-excitons in heavy-fermion semiconductors, J. Magn. Magn. Mater. **226**, 127 (2001).

[28] G. A. Kapilevich, P. S. Riseborough, A. X. Gray, M. Gulacsi, T. Durakiewicz, and J. L. Smith, Incomplete protection of the surface Weyl cones of the Kondo insulator SmB_6: Spin-exciton scattering, Phys. Rev. B **92**, 085133 (2015).

[29] A. Arab, A. X. Gray, S. Nemšák, D. V. Evtushinsky, C. M. Schneider, D. J. Kim, Z. Fisk, P. F. S. Rosa, T. Durakiewicz, and P. S. Riseborough, Effects of spin-excitons on the surface states of SmB_6: A photoemission study, Phys. Rev. B **94**, 235125 (2016).

[30] B. Gorshunov, N. Sluchanko, A. Volkov, M. Dressel, G. Knebel, A. Loidl, and S. Kunii, Low-energy electrodynamics of SmB_6, Phys. Rev. B **59**, 1808 (1999).

[31] S. Gabani, K. Flachbart, E. Konovalova, M. Orendac, Y. Paderno, V. Pavlik, and J. Sebek, Properties of the in-gap states in SmB_6, Solid State Commun. **117**, 641 (2001).

[32] K. Flachbart, S. Gabani, K. Neumaier, Y. Paderno, V. Pavlik, E. Schuberth, and N. Shitselova, Specific heat of SmB_6 at very low temperatures, Physica B Condens. Matter **378-380**, 610 (2006).

[33] W. A. Phelan, S. M. Koohpayeh, P. Cottingham, J. W. Freeland, J. C. Leiner, C. L. Broholm, and T. M. McQueen, Correlation between Bulk Thermodynamic Measurements and the Low-Temperature-Resistance Plateau in SmB_6, Phys. Rev. X **4**, 031012 (2014).

[34] M. Orendáč, S. Gabáni, G. Pristáš, E. Gažo, P. Diko, P. Farkašovský, A. Levchenko, N. Shitsevalova, and K. Flachbart, Isosbestic points in doped SmB_6 as features of universality and property tuning, Phys. Rev. B **96**, 115101 (2017).

[35] J. Stankiewicz, M. Evangelisti, P. F. S. Rosa, P. Schlottmann, and Z. Fisk, Physical properties of Sm_xB_6 single crystals, Phys. Rev. B **99**, 045138 (2019).

[36] Y. Luo, H. Chen, J. Dai, Z.-A. Xu, and J. D. Thompson, Heavy surface state in a possible topological Kondo insulator: Magnetothermoelectric transport on the (011) plane of SmB_6, Phys. Rev. B **91**, 075130 (2015).

[37] G. Li, Z. Xiang, F. Yu, T. Asaba, B. Lawson, P. Cai, C. Tinsman, A. Berkley, S. Wolgast, Y. S. Eo, D.-J. Kim, C. Kurdak, J. W. Allen, K. Sun, X. H. Chen, Y. Y. Wang, Z. Fisk, and L. Li, Two-Dimensional Fermi-surfaces in Kondo insulator SmB_6, Science **346**, 1208 (2014).

[38] Y. Nakajima, P. Syers, X. F. Wang, R. X. Wang, and J. Paglione, One-dimensional edge states in a topological Kondo insulator, Nat. Phys. **12**, 213 (2016).

[39] W. T. Fuhrman, J. R. Chamorrow, P. A. Alekseev, J.-M. Mignot, T. Keller, J. A. Rodriguez-Rivera, Y. Qiu, P. Nikolic, T. M. McQueen, and C. L. Broholm, Screened moments and extrinsic in-gap states in samarium hexaboride, Nat. Commun. **9**, 1539 (2018).

[40] B. S. Tan, Y.-T. Hsu, B. Zeng, M. Ciomaga Hatnean, N. Harrison, Z. Zhu, M. Hartstein, M. Kiourlappou, A. Srivastava, M. D. Johannes, T. P. Murphy, J.-H. Park, L. Balicas, C. G. Lonzarich, G. Balakrishnan, and S. E. Sebastian, Unconventional Fermi-surface in an insulating state, Science **349**, 287 (2015).

[41] M. Hartstein, W. H. Toews, Y.-T. Hsu, B. Zeng, X. Chen, M. Ciomaga Hartnea, Q. R. Zhang, S. Nakamura, A. S. Padgett, G. Rodway-Grant, J. Berk, M. K. Kingston, G. H. Zhang, M. K. Chan, S. Yamashota, T. Sakakibara, Y. Takano, J.-H. Park, L. Balicas, N. Harrison, N. Shitselova, G. Blalakrishnan, G. G. Lonzarich, R. W. Hill, M. Sutherland, and S. E. Sebastian, Fermi-surface in the absence of a Fermi-liquid in the Kondo insulator SmB_6, Nat. Phys. **14**, 166 (2017).

[42] Y. Xu, S. Cui, J. K. Dong, D. Zhao, T. Wu, X. H. Chen, K. Sun, H. Yao, and S. Y. Li, Bulk Fermi Surface of Charge-Neutral Excitations in SmB_6 or Not: A Heat-Transport Study, Phys. Rev. Lett. **116**, 246403 (2016).

[43] M.-E. Boulanger, F. Laliberte, M. Dion, S. Badoux, N. Doiron-Leyraud, W. A. Phelan, S. M. Koohpayeh, W. T. Fuhrman, J. R. Chamorro, T. M. McQueen, X. F. Wang, Y. Nakajima, T. Metz, J. Paglione, and L. Taillefer, Field-dependent heat transport in the Kondo insulator SmB_6: Phonons scattered by magnetic impurities, Phys. Rev. B **97**, 245141 (2018).

[44] N. J. Laurita, C. M. Morris, S. M. Koohpayeh, P. F. S. Rosa, W. A. Phelan, Z. Fisk, T. M. McQueen, and N. P. Armitage, Anomalous three-dimensional bulk ac conduction within the Kondo gap of SmB_6 single crystals, Phys. Rev. B **94**, 165154 (2016).

[45] R. Sollie and P. Schlottmann, A simple theory of the Kondo hole, J. Appl. Phys. **69**, 5478 (1991).

[46] P. S. Riseborough, Collapse of the coherence gap in Kondo semiconductors, Phys. Rev. B **68**, 235213 (2003).

[47] M. E. Valentine, S. Koohpayeh, W. A. Phelan, T. M. McQueen, P. F. S. Rosa, Z. Fisk, and N. Drichko, Breakdown of the Kondo insulating state in SmB_6 by introducing Sm vacancies, Phys. Rev. B **94**, 075102 (2016).

[48] Z. Xiang, B. Lawson, T. Asaba, C. Tinsman, Lu Chen, C. Shang, X. H. Chen, and Lu Li, Bulk Rotational Symmetry Breaking in Kondo Insulator SmB_6, Phys. Rev. X **7**, 031054 (2017).

[49] S. M. Thomas, X. Ding, F. Ronning, V. Zapf, J. D. Thompson, Z. Fisk, J. Xia, and P. F. S. Rosa, Quantum Oscillations in Flux-Grown SmB_6 with Embedded Aluminum, Phys. Rev. Lett. **122**, 166401 (2019).

[50] H. Shen and L. Fu, Quantum Oscillation from In-Gap States and a Non-Hermitian Landau Level Problem, Phys. Rev. Lett. **121**, 026403 (2018).

[51] S. Gheidi, K. Akintola, K. S. Akella, A. M. Cote, S. R. Dunsiger, C. Broholm, W. T. Fuhrman, S. R. Saha, J. Paglione, and J. E. Sonier, Intrinsic Low-Temperature Magnetism in SmB_6, Phys. Rev. Lett. **123**, 197203 (2019).

[52] A. J. Niemi and G. W. Semenoff, Fermion number fractionalization in quantum field theory, Phys. Rep. **135**, 99 (1986).

[53] R. Jackiw and C. Rebbi, Solitons with fermion number 1/2, Phys. Rev. D **13**, 3398 (1976).

[54] J. S. Bell and R. W. Jackiw, A PCAC puzzle: $\pi^0 \to \gamma\gamma$ in the σ model, Nuovo Cimento A **60**, 47 (1969).

[55] H.-Z. Lu, W.-Y. Shan, W. Yao, Q. Nu, and S.-Q. Shen, Massive Dirac fermions and spin physics in an ultra-thin film of a topological insulator, Phys. Rev. B **81**, 115407 (2010).

[56] Y. Zhang, K. He, C.-Z. Chang, C.-L. Song, L.-L. Wang, X. Chen, J. F. Jia, Z. Fang, X. Dai, W. Y. Shan, S. Q. Shen, Q. Niu, X. L. Qi, S. C. Zhang, X. C. Ma, Q. K. Xue, Crossover of the three-dimensional topological insulator Bi_2Se_3 to the two-dimensional limit, Nat. Phys. **6**, 584 (2010).

[57] T. Yoshida, S. Fujimoto, and N. Kawakami, Correlation effects on a topological insulator at finite temperatures, Phys. Rev. B **85**, 125113 (2012).

[58] V. Alexandrov, P. Coelman, and O. Erten. Kondo Breakdown in Topological Kondo Insulators, Phys. Rev. Lett. **114**, 177202 (2015).

[59] J. Friedel, Metallic alloys, Nuovo Cimento Suppl. **7**, 287 (1958).

[60] N. Levinson, On the uniqueness of a potential in a Schroedinger equation for a given asymptotic phase, Kgl. Danske Viedenskab. Selskab, Mat.-fys. Medd. **25**, 1 (1949).

[61] J. Friedel, The distribution of electrons round impurities in monovalent metals, Philos. Mag. **43**, 153 (1952).

[62] J. Friedel, On some electrical and magnetic properties of metallic solid solutions, Can. J. Phys. **34**, 1190 (1956).

[63] P. W. Anderson, Localized magnetic states in metals, Phys. Rev. **124**, 41 (1961).

[64] U. Fano, Effects of configurational interaction on intensities and phase shifts, Phys. Rev. **124**, 1866 (1961).

[65] L. Fu, C. L. Kane, and E. J. Mele, Topological Insulators in Three Dimensions, Phys. Rev. Lett. **98**, 106803 (2007).

[66] It should be noted that in this model, the void has been assigned the vacuum mass so the void is topologically trivial. In particular, the wave function is not required to vanish in the void but can penetrate it. This is to be contrasted with the model of Ref. [67] for a void in a two-dimensional system where the wave function is excluded from the void and, therefore, the states in the void are neither characterized by parity nor mass. Hence, unlike the model being considered here, the void of Ref. [67] is neither topologically trivial nor nontrivial.

[67] W.-Y. Shan, J. Lu, H.-Z. Lu, and S.-Q. Shen, Vacancy-induced bound states in topological insulators, Phys. Rev. B **84**, 035307 (2011).